

# Computational Study on Controlling the Optical Properties of Solar Thermal Fuels

by

Jee Soo Yoo

S.B., Materials Science and Engineering  
Stanford University (2011)

SUBMITTED TO THE DEPARTMENT OF MATERIALS SCIENCE AND ENGINEERING  
IN PARTIAL FULLFILLMENT OF THE REQUIREMENTS FOR THE DEGREE OF  
MASTER OF SCIENCE IN MATERIALS SCIENCE AND ENGINEERING  
AT THE  
MASSACHUSETTS INSTITUTE OF TECHNOLOGY

SEPTEMBER 2019

© 2019 Massachusetts Institute of Technology. All rights reserved

Signature redacted

Signature of Author .....

Department of Materials Science and Engineering  
August 19, 2019

Certified by .....

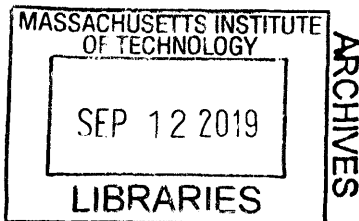
Signature redacted

Jeffrey C. Grossman  
Professor of Materials Science and Engineering  
Thesis Advisor

Signature redacted

Accepted by .....

: Donald R. Sadoway  
John F. Elliott Professor of Materials Chemistry  
Chairman, Departmental Committee on Graduate Studies





# Computational Study on Controlling the Optical Properties of Solar Thermal Fuels

by

Jee Soo Yoo

Submitted to the Department of Materials Science and Engineering on August 19, 2019 in Partial fulfillment of the requirements for the Degree of Master of Science in  
Materials Science and Engineering

## ABSTRACT

Solar thermal fuels utilize molecules that undergo reversible photo-isomerization to convert solar energy into stored thermal energy.<sup>1</sup> Because solar thermal fuels produce no emissions and can store and convert energy within one material, they are an attractive option for a renewable energy source. However, it has remained a challenge to identify a suitable solar thermal fuel material that exhibits high energy density, high energy conversion efficiency, long energy storage lifetime, and can be produced at low cost. A recent proposal is a nanotemplate-photoisomer hybrid system, *e.g.* functionalized azobenzene, a well-known photoisomer molecule, attached to carbon nanostructure templates such as carbon nanotubes, graphene, pentacene or alkene chains. Such structures have been suggested and tested as candidate solar thermal fuel materials with high energy density and long storage time<sup>2-4</sup> In this thesis work, we further investigated optical properties of functionalized azobenzene and geometry-modified azobenzene. We found the best structure that yields maximum optical isomerization rate for trans-azobenzene and minimum optical isomerization rate for cis-azobenzene, calculating the reaction rate based on overlap between the solar spectrum and optical spectra calculated using time-dependent density functional theory (TDDFT). We showed that energy-charged-state molecule (cis-isomer) content at the photostationary state can be improved from 73 percent for pure azobenzene to 83 percent and to 97 percent by functionalizing azobenzene and a designing different geometry for azobenzene, respectively. From this, a desired structure for nanotemplates-photoisomer hybrid system can be estimated and same calculation technique may be employed to calculate and optimize photostationary state of the nanotemplates-photoisomer hybrid system.

Thesis Supervisor: Jeffrey C. Grossman  
Title: Professor of Materials Science and Engineering

# Acknowledgment

I would like to thank my advisor, Jeffrey C. Grossman for supporting my entire graduate work. He always kindly provided insights and guidances for my research as well as for my career. I also want to thank for leading our research group as a cheerful and supportive group not to mention our exciting group retreats and group lunches.

Our group members helped me a lot from the beginning when I had to adapt to various calculation techniques and also inspired me on presenting my data in better form and finding new ideas.

Also, my friends in Boston area has made me enjoy the life in this city a lot. Doing various activities such as attending concerts, musicals, and ballet and

Finally, I would like to thank my family for their love and support. Even though they were mostly far away in Korea, we constantly had video calls and every time they cheered me up when I had difficulties.

# Contents

## **1. Introduction**

1.1 Solar Thermal Fuels

1.2 Previous Solar Thermal Fuel Efforts

1.3 Recent Advances in Azobenzene-Based Solar Thermal Fuels

## **2. Motivation**

2.1 Photostationary State

2.2 Formulating Photostationary State

2.3 Strategies for Photostationary State Engineering

## **3. Azobenzene Functionalization**

3.1 Motivation for Functionalized Azobenzene

3.2 Theoretical Approaches to the Photostationary State of Functionalized Azobenzene

3.2.1 Geometry Optimization of Functionalized Azobenzene

3.2.2 Theoretical Calculation of Optical Spectra of Azobenzene Derivatives

3.3 Photostationary State of Azobenzene Derivatives

## **4. Azobenzene Geometry Modification**

4.1 Motivation for Geometry Modification of Azobenzene

4.2 Rotational Degrees of Freedom

4.3 Storage Enthalpy and Absorption Spectra of Geometry-Modified Azobenzene

## **5. Conclusion**

## List of Figures

Figure 1.1: Four methods developed to harvest solar energy

Figure 1.2: Schematic of solar thermal fuel energy cycle with azobenzene molecule as an example

Figure 1.3: Photoisomerization reactions studied for solar thermal fuel applications

Figure 1.4: CNT-templated Azo STF Schematics and chemical structure

Figure 1.5: Combinations of nano-templates and azobenzene derivatives

Figure 1.6: Optical and thermal cycles of SWCNT-Azo STF

Figure 1.7: Inter-template interaction of SWCNT-Azo STF

Figure 1.8: Graphene/RGO-templated Azo STF chemical structures

Figure 3.1: Schematic diagram of azobenzene functionalization with all studied functional groups

Figure 3.2: Comparison between experimentally measured and theoretically calculated spectra of (a) trans-azobenzene and (b) cis-azobenzene

Figure 3.3: Ionization of benzoic acid with substituents  $R$  and  $R'$  on para- and meta-position, respectively.

Figure 3.4: Absorption spectra of trans- and cis-azobenzene with  $-NH_2$  substitution at para-position

Figure 3.5: Absorption spectra of trans- and cis-azobenzene with  $-NO_2$  substitution at para-position

Figure 3.6: Photostationary state molar fraction  $x_{cis}$  with respect to the storage enthalpy  $\Delta H$

Figure 3.7: Photostationary state molar fraction  $x_{cis}$  with respect to the Hammett constant  $\sigma$ .

Figure 3.8: Integrated volume around N=N double bond.

Figure 3.9: Correlation between extra number of electrons in N=N bond  $\Delta N_{N=N}$  and the Hammett constants  $\sigma$

Figure 3.10: Photostationary state cis-isomer molar fraction  $x_{cis}$  in function of # of extra N=N electrons  $\Delta N_{N=N}$ .

Figure 4.1: Rotational degrees of freedom of trans-azobenzene and cis-azobenzene

Figure 4.2: Ground-state energy surface of (a) trans- and (b) cis-azobenzene in function of geometry.

Figure 4.3: Absorption Spectra of trans-azobenzene with different geometry

Figure 4.4: Absorption Spectra of cis-azobenzene with different geometry

Figure 4.5: Peak positions of geometry-modified trans- and cis-azobenzene in color map

Figure 4.6: Peak intensities of geometry-modified trans- and cis-azobenzene in color map

Figure 4.7: Optical isomerization rate of geometry-modified trans-azobenzene and cis-azobenzene

Figure 4.8: Extra number of electrons on N=N double bond of trans-azobenzene and optical isomerization rate of trans-azobenzene in function of extra number of N=N electrons

Figure 4.9: Extra number of electrons on N=N double bond of trans-azobenzene and optical isomerization rate of cis-azobenzene in function of extra number of N=N electrons

## List of Tables

Table 1.1: Energy density, half-life, phase change and grafting density of graphene/RGO templated-Azo STFs

Table 2.1: Molar fractions and reaction rates at ideal ground state, ideal storage state, photostationary state and real storage state

Table 3.1: Internal quantum efficiency of photoisomerization for trans- and cis-azobenzene.



# Chapter 1

## Introduction

Solar energy has drawn wide attention as the alternative energy source that can overcome the depletion and the global warming side effect of traditional fossil fuels. Especially, the abundance of solar energy is attractive since 40,000 TWy of solar energy arrives on earth every year while the world energy consumption is 18.5TWy as of 2015.<sup>5</sup> However challenges remain in converting solar energy into usable energy and storing it.

Figure 1.1 shows four prevalent ways developed for harvesting solar energy, namely photovoltaics, artificial photosynthesis, concentrated solar thermal power, and solar thermal fuels. Photovoltaics (PVs), or solar cells convert optical energy directly into electrical energy. So far, PVs are the most utilized method to collect solar energy.<sup>6</sup> They can collect both direct light and diffuse light. PVs can be used as a stand-alone device or connected to grid or electrical energy storage system (ESS). Since solar cells can only produce electricity when the Sun is present, grid system or ESS manages the distribution of energy.<sup>6</sup> Concentrated Solar Power (CSP), or solar

thermal technology, uses mirrors to concentrate solar energy to a tower as shown in Figure 1.1(b). The concentrated solar energy heats up a phase change material on top of the tower. The phase change material thus converts solar energy into thermal energy and then to chemical energy. The phase change material then releases its heat to produce electricity on the lower part of the tower, converting the chemical energy into electrical energy. Since the heated phase change material can be stored for some time (~ a few days), it can be utilized to produce energy when there is no Sun. Therefore, CSP can produce electricity in more stable manner. Overall energy production cost is also cheaper for CSP plant than for PV when installed in large areas in low latitude, but CSP requires cleaning the mirrors and managing the angles which requires additional manpower.<sup>6</sup> Figure 1.1(c) shows artificial photosynthesis that mimics botanical photosynthesis that synthesizes carbohydrates or produce hydrogen gas using solar energy. Again, the solar energy is converted into chemical energy. The carbohydrates can then release energy either through hydrolysis or direct combustion. Here, the storage and transport of the produced fuels can be challenges for wide use.<sup>7</sup> Figure 1.1(d) shows an example mechanism of a solar thermal fuel, in this case carbon nanotube templated-azobenzene. Solar thermal fuel materials undergo photoisomerization under sunlight, thus converting solar energy into chemical energy. It can store energy within the material itself and can be transferred to where it is needed. When triggered, the solar thermal fuel releases heat energy as the material isomerizes back to ground state.

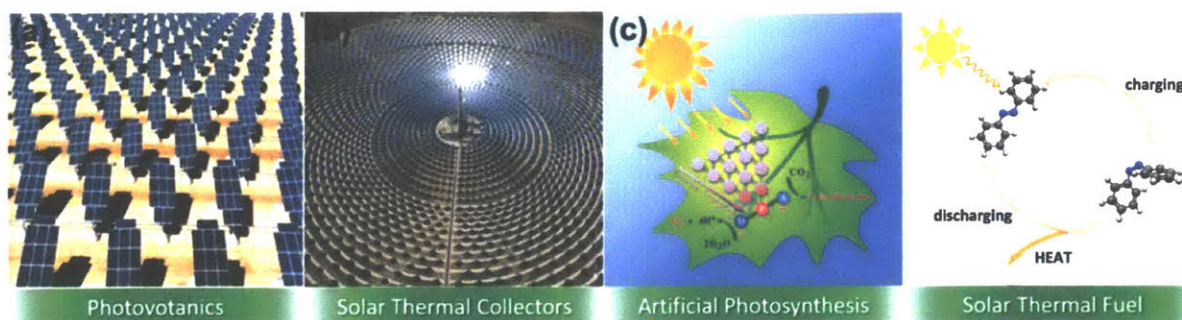


**Figure 1.1** | Four methods developed to harvest solar energy: (a) photovoltaics, (b) solar thermal collectors, (c) artificial photosynthesis and (d) solar thermal fuel. Figure taken from Dong, L., *et al. Chem. Soc. Rev.* **47**, 7339–68 (2018).<sup>8</sup>

## 1.1 Solar Thermal Fuels

Weigart first suggested the idea of a solar thermal fuel (STF), collecting solar energy in sterically strained chemical bonds in 1909 after observing the photoconversion of anthracene crystals under sunlight.<sup>9</sup> Solar thermal fuels have many potential advantages as solar energy harvesting and storing system. As Figure 1.2 shows, solar thermal fuels use closed cycle reactions and hence produce no emission. Also, since STFs convert and store energy within one material, they can be used in transportable small-scale devices. Moreover, by tuning the activation energy barrier of the backward reaction, the storage lifetime can be elongated to achieve long-term energy storage.<sup>1</sup>

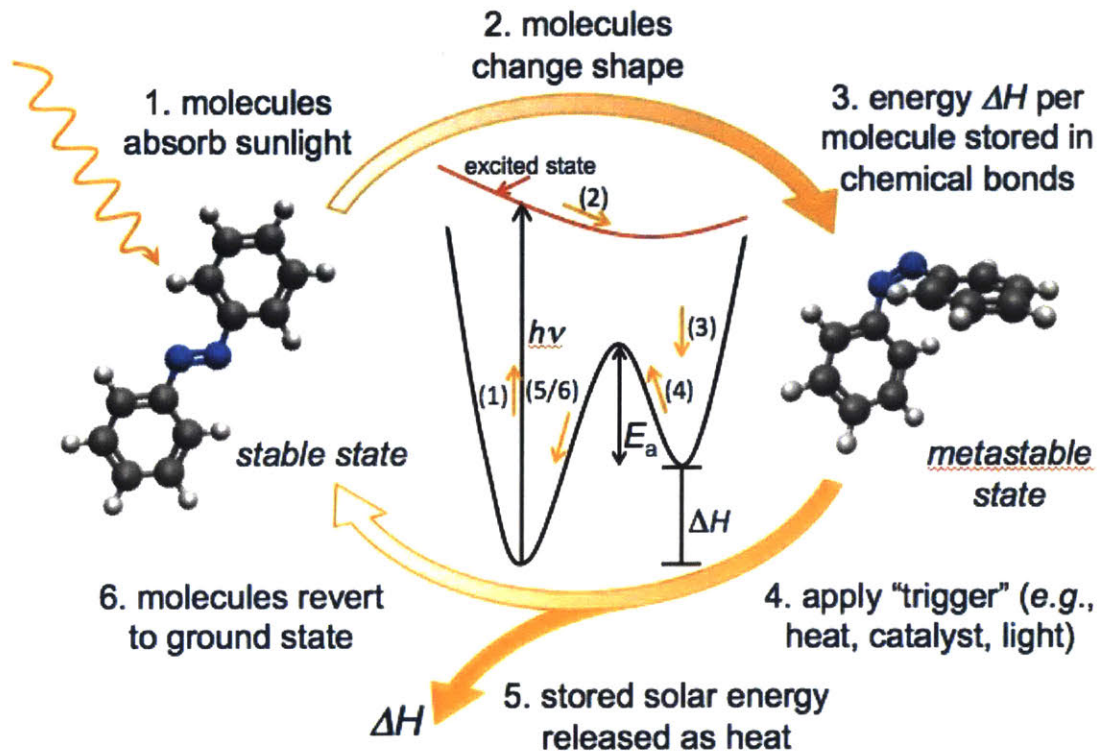


**Figure 1.2** | Schematic of solar thermal fuel energy cycle with azobenzene molecule as an example. When a molecule absorb sunlight, the molecule is excited to the excited state and changes shape (photoisomerization) along the excited state energy surface. Eventually the molecule comes back to ground state energy surface, i.e. metastable state which corresponds to the local minima of energy surface. When a “trigger” that is enough to overcome the activation energy barrier  $E_a$  is applied, the molecule reverts back to the ground state and the stored energy, i.e. enthalpy difference  $\Delta H$  is released.

The requirements for a solar thermal fuel system to be a practical energy technology have been analyzed with the following key objectives.<sup>10–13</sup> For STF’s ground state structure A and metastable structure B,

- 1) The absorption spectra of substance A and B should line up with the solar spectrum such that A absorbs strongly in the 300–700 nm region (in which more than 50 percent of solar energy reaches the Earth) while B absorbs only slightly in this region;

2)  $\Delta H$ , the amount of heat released per molecule in the back reaction  $B \rightarrow A$  should be large so that the volumetric and gravimetric energy densities of the system are competitive with other commercial energy storage systems.

3) The activation energy  $E_a$  of the thermal back reaction  $B \rightarrow A$  must be large enough so that the lifetime of the metastable state B ensures prolonged duration of storage.

4) There should be a trigger, which may be catalytic, thermal, electrical, or optical, that accelerates the heat release reaction  $B \rightarrow A$  near room temperature; preferably not higher than 50-100 degrees Celsius;

5) The internal quantum efficiency of the forward reaction  $A \rightarrow B$ , i.e., the probability that an absorbed photon leads to the photochemical reaction, should be high and both A and B should not have luminescence. Therefore, intramolecular reactions are preferred to intermolecular reactions, which in general have low quantum yield;

6) There should be an absence of side-reactions that produce by-products in either forward or reverse reactions;

7) Safety of the system should be ensured and substance A and B should be inexpensive.

## 1.2 Previous Solar Thermal Fuel Efforts

Over the years, researchers have tested various photoisomers as solar thermal fuels.

Figure 1.3 shows six prominent photoisomerization reactions among those. Anthracene photodimerizes through cycloaddition under UV light around 400nm wavelength.<sup>9,11</sup> The energy stored through this reaction,  $\Delta H$ , is 65.2 kJ/mol or 0.676 eV for pure anthracene.<sup>9</sup> By

functionalizing the anthracene molecule with electron donating groups (EDGs) and electron withdrawing groups (EWGs), the storage enthalpy could be increased to 83.6 kJ/mol or 0.866 eV. However, the quantum efficiency of the photodimerization depends on the concentration of anthracene molecules and also the upper limit of the quantum efficiency was calculated to be 0.2 to 0.3 by extrapolation of experimental results.<sup>14,15</sup>

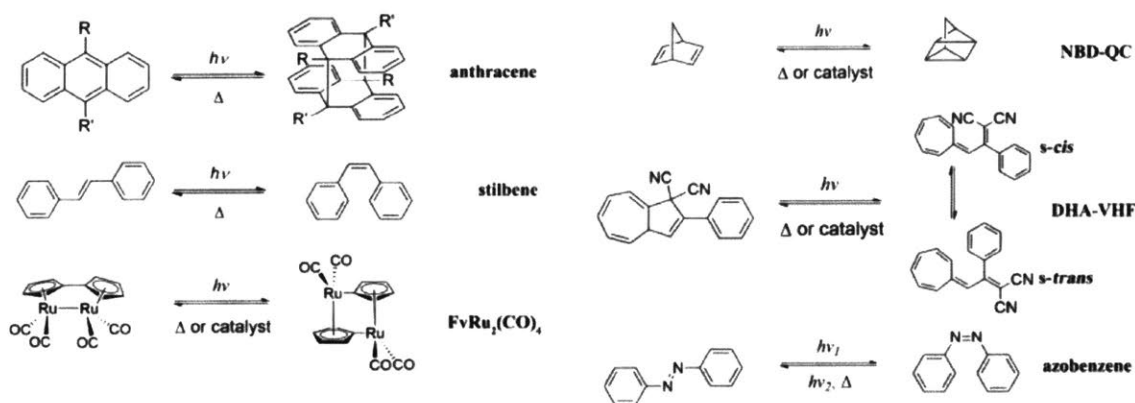


**Figure 1.3** | Photoisomerization reactions studied for solar thermal fuel applications. Figure taken from Dong, L., *et al. Chem. Soc. Rev.* **47**, 7339–68 (2018).<sup>8</sup>

Stilbene photoisomerizes between trans- and cis-structure under visible light ranging from 300 nm to 700 nm.<sup>16</sup> The simple inversion and rotation mechanism of the photoisomerization leads to the stability against side reactions.<sup>1,17</sup> Also, stilbene can be synthesized in low cost and has low molecular weight. However, the storage enthalpy is about 5 kJ/mol (0.052 eV) and hence limited for solar thermal fuel usage.<sup>16</sup> Functionalizing the phenyl ring of stilbene with functional groups such as methylstyryl group and naphthyl group could increase the storage enthalpy to 1.07 eV.<sup>16,18,19</sup>

Tetracarbonyl (fulvalene) diruthenium ( $\text{FvRu}_2(\text{CO})_4$ ) is also a thoroughly studied material for solar thermal fuels. The organometallic complex photoisomerizes under visible light

(350nm to 470nm) and the storage enthalpy is 125 kJ/mol (1.29 eV).<sup>20-24</sup> The high molecular weight of ~442 g/mol and the high cost of Ru metal as the raw material, however, undermines the potential of fulvalene diruthenium for solar thermal fuel applications. Therefore, different metals such as iron (Fe), osmium (Os) and molybdenum (Mo) were tested to replace Ru, but Fe and Mo analogues failed to photoisomerize and the Os analogue could photoisomerize but not reversibly.<sup>25-27</sup>

Norbornadiene (NBD) and quadricyclane (QC) photoisomerization pair have been studied the most due to: (1) its engineering flexibility because of the liquid forms of both compounds at room temperature, (2) low cost synthesis through Diels-Alder reactions, (3) high energy density (1190 J/g) with  $\Delta H=1.0\text{eV}$ , (4) readiness of triggering the back-reaction using transition-metal complex catalysts and (5) negligible quantum efficiency of the photochemical back-reaction.<sup>28-33</sup> The major drawback of this system as a solar thermal fuel is that norbornadiene absorbs at short wavelengths about 300nm and hence has a small overlap with solar spectrum.<sup>31-33</sup> To red-shift the absorption spectrum of norbornadiene, functionalized norbornadiene and mixtures with sensitizers have been tested and showed red shift up to ~365 nm and ~546 nm, respectively.<sup>30,33</sup> Another drawback of NBD-QC system is the cyclability: NBD is prone to polymerize and form explosive peroxides in the presence of air and light.<sup>32</sup>

Dihydroazulene (DHA) photoisomerizes to vinylheptafulvene (VHF) through a ring-opening reaction under ~350 nm UV light.<sup>34-41</sup> The stored enthalpy is 27.7 kJ/mol (0.287 eV) which leads to an energy density of 0.11 MJ/kg.<sup>36,39</sup> The energy density can be increased to 0.36 MJ/kg by replacing the benzene ring of DHA to a naphthalene ring.<sup>40</sup>

Trans-azobenzene (trans-Azo) absorbs UV light around 365 nm and photoisomerizes into cis-azobenzene (cis-Azo).<sup>42-44</sup> The stored enthalpy and the half-life of cis-Azo were reported

to be 49 kJ/mol (0.51 eV) and 4.2 days, respectively. Cis-Azo can either thermally or photochemically revert back to trans-Azo and the backward and forward reaction can be repeated with almost no degradation.<sup>43,45</sup> Similar to stilbene which also undergoes a trans-cis isomerization, azobenzene also has the advantage for its low-cost synthesis. However, the small storage enthalpy and thus low energy storage capacity as well as the high quantum efficiency of the back photochemical reaction (i.e. from cis-isomer to trans-isomer) have hindered the practical use of azobenzene for solar thermal fuels. Moreover, a longer lifetime of the metastable charged state (on the order of >weeks) is desired for most applications.

## 1.3 Recent Advances in Azobenzene-Based Solar Thermal Fuels

Kolpak et al. recently suggested photoisomer and nano-template hybrid structures as a novel approach to design solar thermal fuel as shown in Figure 1.4.<sup>2,3</sup> Calculations were performed for functionalized azobenzene molecules covalently attached to nanotemplates such as carbon nanotube (CNTs), graphene, alkene chains, pentacene, fullerene and  $\beta$ -carotene as shown in Figure 1.5.<sup>2,3</sup> The advantage of introducing the nano scale templates is that volumetric energy density increases since the photoswitches are packed in small volume and a systematic manipulation of the inter- and intramolecular interactions of the photoisomerization centers is enabled in a new ordered phase. Using density functional theory,  $\Delta H$  and  $E_a$  were computed for various combinations of photoisomers and templates and it was shown that  $\Delta H$  and  $E_a$  could be



as high as 1.8eV and 1.6eV, respectively. These values correspond to the heat release temperature of 750K, energy density of 0.803 MJ/kg and storage lifetime of  $10^8$  days. These theoretical works showed promising characteristics for new azobenzene-based molecular designs for solar thermal fuels.

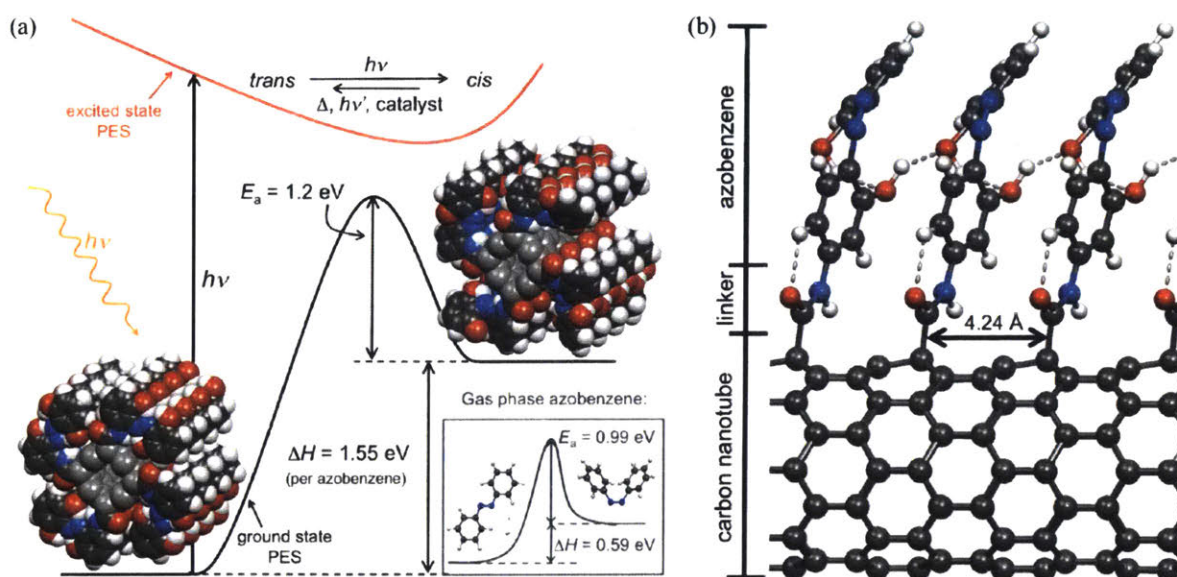


**Figure 1.4 | CNT-templated Azo** (a) Schematic diagram shows the solar thermal fuel mechanism on potential energy surfaces. On left, 2,2',5'-tridroxy diazobenzene molecules are templated on a carbon nanotube (CNT) is at the ground state. The templated-Azo in trans-structure absorbs photon and becomes excited state. The molecule gets relaxed on the excited state potential energy surface (PES) and finally reaches the metastable state, i.e. cis-structure. The enthalpy difference  $\Delta H = 1.55$  eV is stored in the metastable state solar thermal fuel. To release this energy, activation energy barrier  $E_a = 1.2$  eV should be overcome by triggering heat or light. Compare to the gas phase azobenzene, the energy stored per azobenzene increased by 2.6 times and the activation energy increased by 1.2 times, leading to higher energy density and longer storage lifetime, respectively. (b) Side view of CNT templated only on one row with azobenzene derivatives, 2,2'-dihydroxy-diazobenzene. Azobenzene derivatives are attached to CNT via amide linker groups at the para-position of azobenzene. Dotted lines indicate hydrogen bonding within the structure. Figure taken from Kolpak, A. M. & Grossman, J. C. *Nano Lett.* 11, 3156–3162 (2011).<sup>2</sup>

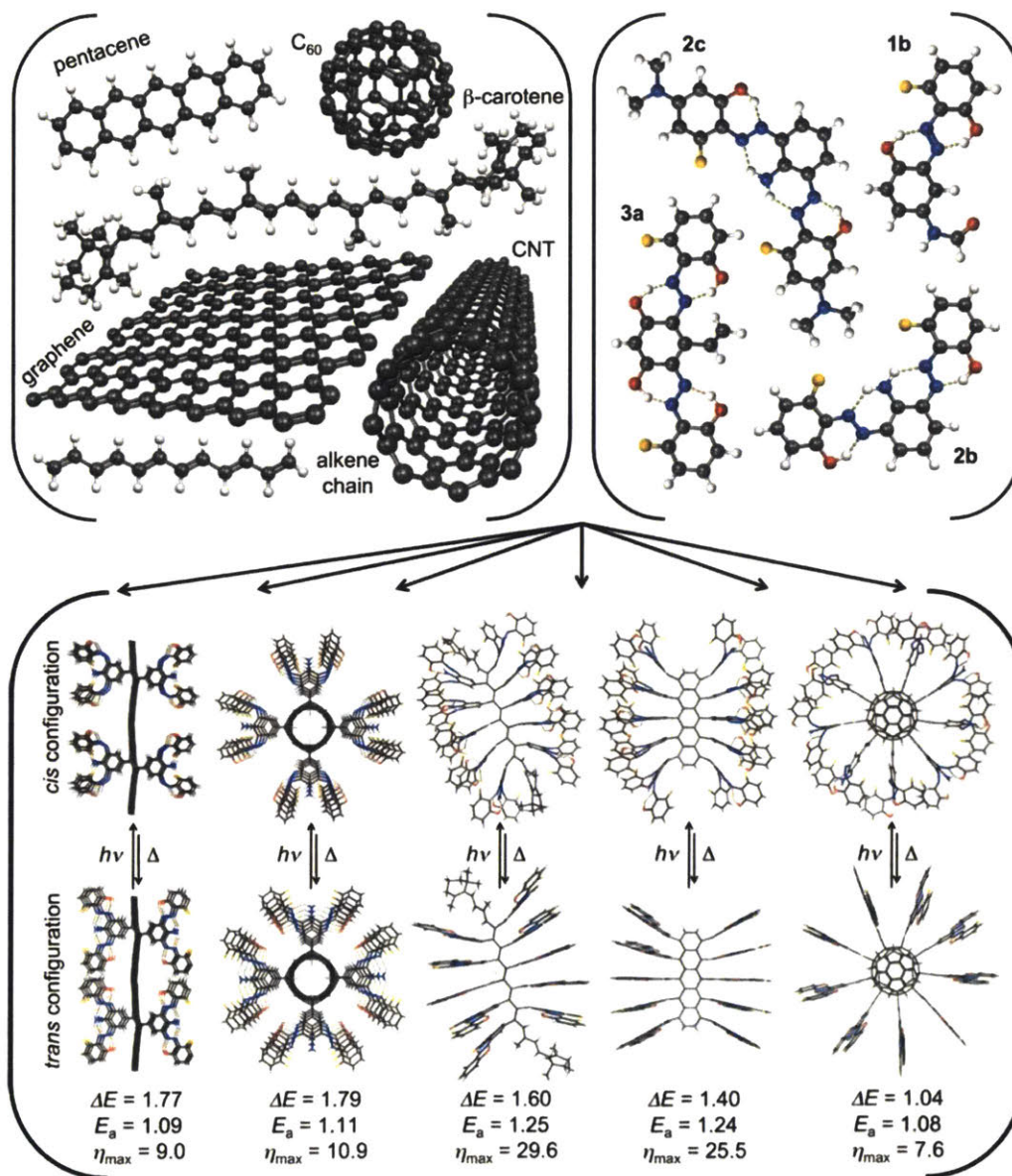


**Figure 1.5** | Upper left corner lists nanotemplates materials and the upper right corner shows various functionalized azobenzene molecules. White, dark gray, blue, red, and orange balls represent H, C, N, O, and F atoms, respectively. The bottom part shows trans/cis configuration of templated-Azo system and its properties such as energy difference  $\Delta E$  between trans/cis configuration, activation energy barrier  $E_a$ , and maximum external efficiency  $\eta_{max}$ . Figure taken from Kolpak, A. M. & Grossman, J. C. *J. Chem. Phys.* 138, 034303 (2013).<sup>3</sup>

Inspired by such theoretical works, many azobenzene-based molecular designs were synthesized and tested for solar thermal fuel applications. Kucharski *et al.* synthesized single-wall carbon nanotube (SWCNT) and tested photochemical and thermal isomerization cycles.<sup>4</sup> As shown in Figure 1.6, both optical cycling and thermal cycling showed no degradation over 2000 cycles. Using differential scanning calorimetry (DSC), the bulk gravimetric energy density of the SWCNT-azobenzene material was measured to be 0.20 MJ/kg (56 Wh/kg) in the solid state. This gravimetric energy density decreased to 0.16 MJ/kg (44 Wh/kg) when diluted suggesting the formation of inter-template interactions as shown in Figure 1.7(a). Theoretical studies using density functional theory on the inter-template interactions showed a large impact on  $\Delta H_{cis-trans}$  for less than 2.4 nm of CNT-CNT distance as shown in Figure 1.7(b).

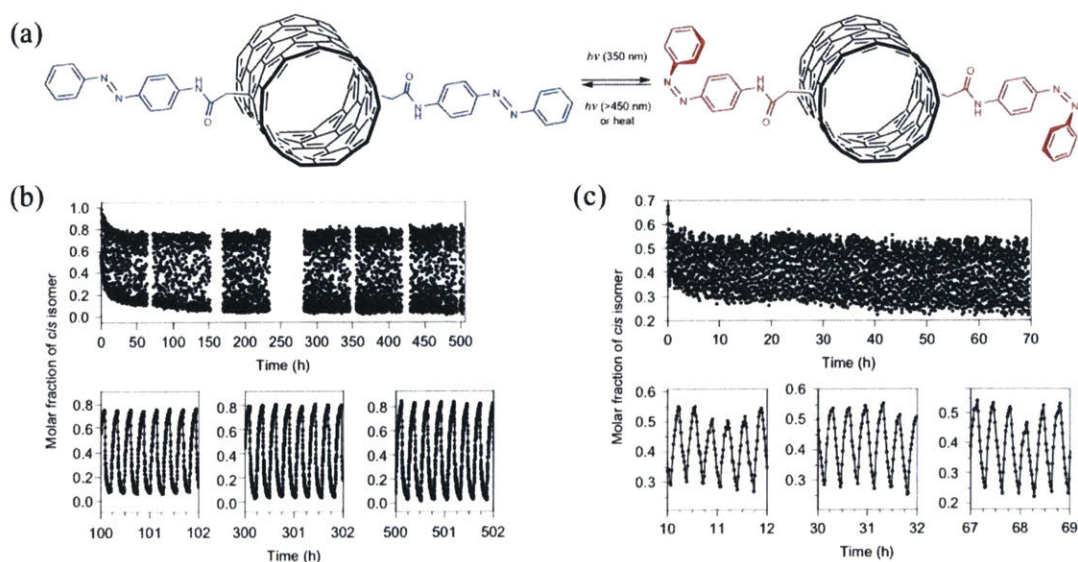


**Figure 1.6** | (a) Schematic illustration of SWCNT-azobenzene covalently bonded with amide group linker. For charging (i.e. isomerization from trans- to cis-isomer), 350 nm light was shined and for discharging,  $\geq 450$  nm light was shined for optical cycles (b) and the sample was held at 75 °C. Figure was taken from Kucharski, T. J. *et al. Nat. Chem.* **6**, 441–447 (2014).

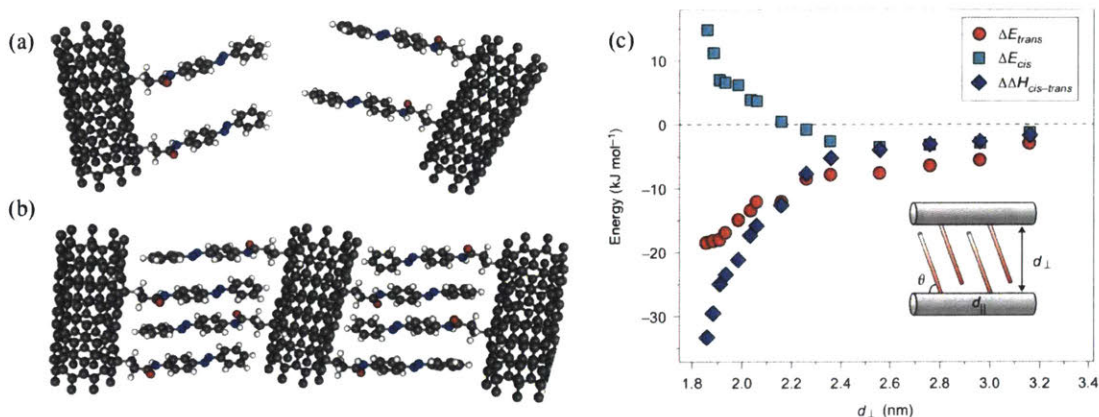


**Figure 1.7** | Illustration of (a) diluted SWCNT-Azo in a suspension and (b) solid-state SWCNT-Azo with significant interaction between template-Azo units. (c) The effect of template-template distance  $d_{\perp}$  on the enthalpy difference between cis- and trans-isomers  $\Delta H_{cis-trans}$ . Figure was taken from Kucharski, T. J. *et al. Nat. Chem.* **6**, 441–447 (2014).

Feng and co-workers extensively studied graphene and reduced graphene oxide (RGO) as the nanotemplates for azobenzene isomers as listed in Figure 1.8.<sup>46–50</sup> Graphene and RGO templated-Azo STF also showed increased energy density and half-life as shown in Table 1.1. The maximum energy density 497 J/g (0.497 MJ/kg) was achieved with structure Figure 1.8(e) and the maximum half-life 5408 h was achieved with structure 1.7(a). The inter-template interaction was also observed in graphene-templated Azo.

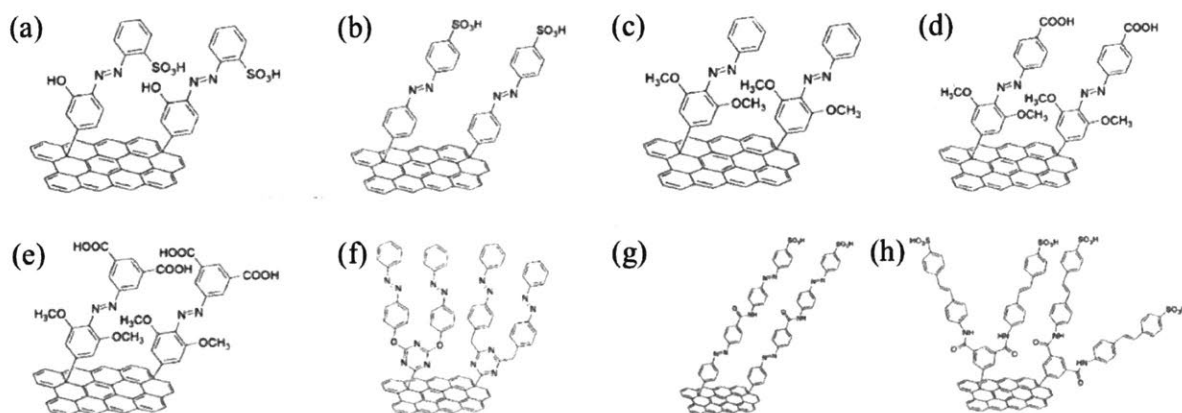


**Figure 1.8** | List of graphene/RGO templated Azo STFs tested. The properties of these materials are listed in Table 1.1. Figure taken from Dong, L., *et al. Chem. Soc. Rev.* **47**, 7339–68 (2018).<sup>8</sup>

**Table 1.1** | Energy density, half-life, phase change and grafting density of graphene/RGO templated-Azo STFs. Grafting density indicates the ratio of attached azobenzene molecule per carbon atoms on the template. Table taken from Dong, L., *et al. Chem. Soc. Rev.* **47**, 7339–68 (2018).<sup>8</sup>

Nanocarbon-templated Azo-STFs	Energy density			$\tau_{1/2}$ (h)	State	Grafting density	Ref.
	(kJ mol <sup>-1</sup> )	(J g <sup>-1</sup> )	(W h kg <sup>-1</sup> )				
a	60 <sup>a</sup>	151	42	5408	Liquid ↔ solid	1/10	44
b	103 <sup>a</sup>	270	75	116	Liquid ↔ solid	1/10	44
c	118	245	68	2	Liquid ↔ solid	1/19	45
d	192	403	112	792	Liquid ↔ solid	1/16	46
e	265	497	138	1248	Liquid ↔ solid	1/17	47
f	318 <sup>a</sup>	288	80	1320	Liquid ↔ solid	1/50	48
g	412 <sup>a</sup>	346	96	1120	Solid	1/59	48
h	572 <sup>a</sup>	472	131	900	Solid	1/46	48

<sup>a</sup> The mole-energy density (kJ mol<sup>-1</sup>) is calculated through multiplying  $M_n$  (g mol<sup>-1</sup>) and mass-energy density (J g<sup>-1</sup>), where  $M_n$  is the molecular weight of azobenzene compounds.

More molecular designs synthesized and tested for azobenzene-based STFs include polymer-templated Azo,<sup>51,52</sup> liquid crystal structure,<sup>51,53</sup> and phase-change material (PCM) doping.<sup>54</sup>

# Chapter 2

## Motivation

Recent developments in azobenzene-based solar thermal fuels enhanced bulk gravimetric energy density and storage lifetime considerably while still maintaining the cyclability. However, there is room for development in the photochemistry of Azo-based STFs, namely, photostationary state, to enhance energy density and charging rate of solar thermal fuels.

## 2.1 Photostationary State

Table 2.1 shows the molar fractions and reaction rates of STFs at ideal discharge state, ideal storage state, photostationary state and real storage state. Molar fractions are defined by

$$x_i = \frac{\text{Number of } i \text{ Molecules}}{\text{Total Number of Molecules}} \quad (2.1)$$

and the reaction rates are defined by

$$v_{forward} = k_{forward}[\text{ground state}], v_{backward} = k_{backward}[\text{metastable state}] \quad (2.2)$$

where  $k_{forward}$  and  $k_{backward}$  are the reaction rate constants of forward and backward reactions, respectively. In the ideal discharge state of the STF, all molecules are at the ground state ( $x_{gs} = 1$ ) and there should be no isomerization reaction ( $v_{forward} = 0, v_{backward} = 0$ ). The discharged STF can then be charged under light through the forward reaction, i.e., photoisomerization reaction from ground state to metastable state. When charging is done, the STF in an ideal storage state should only have metastable state molecules (i.e.  $x_{metastable} = 1$ ). Since the charging is complete, there should be no more isomerization reaction ( $v_{forward} = 0, v_{backward} = 0$ ).

However, such an ideal performance is not achieved in realistic STF materials. Since metastable state molecules can also absorb photons and photoisomerize back into ground state molecules, forward and backward reactions compete against each other such that the charging rate decreases from  $v_{forward}$  to  $v_{forward} - v_{backward}$ . Then, when the two rates are equal,  $x_{metastable}$  no longer changes.

This state is called the photostationary state (PSS). When the STF is charged from a complete discharge state to the PSS, the molar fraction of metastable molecules  $x_{metastable}$  asymptotically reaches its maximum value  $x_{PSS}$ , which is less than 1. Among all STF molecules, only metastable state molecules can store energy and hence the harvested energy in PSS is  $1 - x_{PSS}$  less than the ideal state. The real storage state in the fourth column of Table 2.1 indicates STF that is no longer charged and stored in a dark place before energy usage. Depending on the half-life of metastable state molecule, the backward reaction occurs slowly, decreasing the  $x_{metastable}$ .

**Table 2.1** | Molar fractions and reaction rates at ideal discharge state, ideal storage state, photostationary state and real storage state.  $x_{gs}$  stands for ground state molar fraction,  $x_{metastable}$  stands for metastable state molar fraction,  $v_{forward}$  stands for reaction rate from ground state to metastable state and  $v_{backward}$  stands for reaction rate from metastable state to ground state.

	Ideal Discharge State	Ideal Storage State	Photostationary State	Real Storage State
$x_{gs}$	1	0	$1 - x_{PSS}$	$1 - x_{metastable}$
$x_{metastable}$	0	1	$x_{PSS}$	$x_{metastable} (< x_{PSS})$
$v_{forward}$	0	0	$v_{forward}$	$v_{forward}$
$v_{backward}$	0	0	$v_{backward} (= v_{forward})$	$v_{backward} (> v_{forward})$

From the above discussion, we can find two major impacts of the PSS on STF performance: (i) energy stored in STF is decreased by the ratio  $1 - x_{PSS}$  and (ii) the charging rate is decreased to  $v_{forward} - v_{backward}$ . Kucharski et al. reported that in their optical cycling of SWCNT-Azo STF which is shown in Figure 1.5(b), the charged state had about  $x_{cis} = 0.8$ .<sup>4</sup> Also, it took about 60 hours until the sample reached stable span where the maximum and minimum values of  $x_{cis}$  become constant due to the short irradiation cycle that allowed little time to establish a full photostationary state.<sup>4</sup> Such experimental observations demonstrate the importance of PSS on energy storage density and cycling of STF.



## 2.2 Formulating Photostationary State

Let us formulate an expression for the photostationary state molar fraction  $x_{PSS}$  in terms of the solar spectrum and material properties. Let the number of ground state molecules be  $N_{gs}$  and metastable molecules to be  $N_{metastable}$ . Then, equation (2.2) can be re-written as

$$v_{forward} = -k_{forward} \left( \frac{N_{gs}}{V} \right) = -k_{forward} \frac{N}{V} x_{gs} \quad (2.3)$$

$$v_{backward} = -k_{backward} \left( \frac{N_{metastable}}{V} \right) = -k_{backward} \frac{N}{V} x_{metastable} \quad (2.4)$$

where N is the total number of molecules and V is the total volume of STF. The charging rate is then,

$$\text{charging rate} = v_{forward} - v_{backward} = \left( \frac{N}{V} \right) (-k_{forward} x_{gs} + k_{backward} x_{metastable}) \quad (2.5)$$

At the photostationary state, the charging rate is zero. Therefore, by rearranging the equation (2.5) and plugging in  $x_{gs} + x_{metastable} = 1$ , we obtain

$$x_{metastable,PSS} = \frac{k_{forward}}{k_{forward} + k_{backward}} \quad (2.6)$$

The reaction rate constants  $k_{forward}$  and  $k_{backward}$  can be obtained from the overlap integrals of the solar spectrum and absorption spectra of the ground state and metastable state photoisomers.

That is,

$$k_{forward} = \int \frac{I(\lambda) \alpha_{gs}(\lambda) \eta_{gs}(\lambda)}{\frac{hc}{\lambda}} d\lambda \quad (2.7)$$

$$k_{backward} = \int \frac{I(\lambda)\alpha_{metastable}(\lambda)\eta_{metastable}(\lambda)}{\frac{hc}{\lambda}} d\lambda \quad (2.8)$$

where  $I(\lambda)$  is solar spectrum,  $\alpha_i(\lambda)$  is absorption spectrum of material in state  $i$  and  $\eta_i(\lambda)$  is internal quantum efficiency (i.e. probability that isomerization reaction occurs per absorbed photon). Therefore,  $x_{metastable,PSS}$  can be obtained if we know absorption spectra and internal quantum efficiencies of ground state and metastable state molecule using equations (2.6), (2.7) and (2.8).

## 2.3 Strategies for Photostationary State Engineering

Equation (2.6) indicates that the higher the forward reaction rate, the larger the molar fraction  $x_{metastable,PSS}$  at the photostationary state; and the lower the backward reaction rate, the larger the  $x_{metastable,PSS}$ . Therefore, the strategy of PSS engineering is to maximize forward reaction rate  $k_{forward}$  and to minimize backward reaction rate  $k_{backward}$ . To maximize  $k_{forward}$ , the overlap integral of the solar spectrum and ground state molecule absorption spectrum needs to be increased and the quantum efficiency should be enhanced. Since pure trans-azobenzene has its absorption maximum at 365 nm UV light, a red-shift of the absorption peak of the trans-Azo-based isomer (i.e. ground state isomer) toward the visible regime and peak intensity increase is desired to increase the overlap integral and hence the  $k_{forward}$ . To minimize  $k_{backward}$ , the opposite strategy is used: the overlap integral of the solar spectrum and metastable state molecule

absorption spectrum should be reduced and the quantum efficiency should be quenched.

Therefore, for the metastable state molecule, a reduced absorption peak intensity and blue-shift of the peak position is desired.

# Chapter 3

## Azobenzene Functionalization

### 3.1 Motivation for Functionalized Azobenzene

A functional group is a group of atoms in molecules that exhibit characteristic properties. A functional group is covalently bonded to the rest of the molecule. It can be a reaction center itself; or it can affect the electronic structure of the molecule when it substitutes a hydrogen atom linked to carbon on the “parent” molecule. Functional groups can be distinguished into electron donating groups (EDGs) and electron withdrawing groups (EWGs) depending on their effect on the molecule compared to a hydrogen atom. The combination of inductive and resonance effects collectively determine whether a functional group is an EDG or an EWG. An inductive effect polarizes the covalent  $\sigma$ -bond due to the difference in electronegativity of the atoms involved in the bond.<sup>55</sup> Nitrogen, oxygen, sulfur and halogens exhibit an electron-withdrawing inductive effect due to their high electronegativity.<sup>56-58</sup> Resonance effects are due to the delocalization of  $\pi$ -electrons along conjugated  $\pi$ -bonding between the functional group and the rest of the molecule.<sup>59</sup> When attached to a  $sp^2$ -conjugation system such as in the case of a benzene ring,

functional groups with lone pair electrons such as  $\text{-OH}$ ,  $\text{-NH}_2$ , and halogens exhibit an electron-donating resonance effect. The total electron-donating or electron-withdrawing character is the combination of these two effects.

Functionalization (i.e. attaching functional groups on basic STF molecules) has been widely employed to improve STF performance. Anthracene functionalization with EDGs and EWGs increased the storage enthalpy from 65.2 kJ/mol to 83.6 kJ/mol.<sup>11</sup> Stilbene storage enthalpy also increased from  $\sim 5$  kJ/mol to 104 kJ/mol by introducing the 1-naphthyl group instead of phenyl group.<sup>18,19</sup> Functionalizing stilbene with methyl groups also showed a  $\sim 30$  nm red-shift in the spectra and significant absorption peak intensity change.<sup>16</sup> Introducing EWGs on norbornadiene (NBD) red-shifted the absorption peak to  $\sim 460$  nm of NBD as well.<sup>60</sup> Azobenzene derivatives were also studied to achieve high energy density and more overlap with the solar spectrum (i.e. red-shift of absorption spectra).<sup>61,62</sup> For templated-Azo systems, an amide group was used as a linker between azobenzene molecule and templates as shown in Figure 1.4, Figure 1.5, and Figure 1.6.<sup>3,4</sup> Further functionalization on the azobenzene molecule shown in Figure 1.5 and Figure 1.7 enhanced energy density and half-life of STFs by inter-molecular interactions such as hydrogen bonding between the functional groups.<sup>3,4,46-50</sup>

The history in functionalized STFs motivated my theoretical study on functionalizing azobenzene molecules. Functionalization affects absorption spectra of various STF molecules and hence their photostationary state. Since functionalization also affects important STF figure of merits such as the storage enthalpy and the lifetime, a systematic theoretical study on the effect of the functionalization on the photostationary state is desired to optimize STF design. The theoretical study may be validated with previous experimental studies on functionalized azobenzene absorption spectra.

## 3.2 Theoretical Approaches to the Photostationary State of Functionalized Azobenzene

### 3.2.1 Geometry Optimization of Functionalized Azobenzene

Figure 3.1 shows all azobenzene derivatives that are theoretically studied by calculating optical spectra and  $x_{metastable.PSS}$ . Not only functional groups, but also the functionalization positions, i.e., ortho-, meta-, and para-functionalization are also known to affect chemical properties due to the different corresponding resonance effects. Therefore, all three functionalization positions are tested for each functional group.

The functional groups are chosen such that (1) the amide group which was an important linker group in CNT-Azo systems must be included,<sup>3,4</sup> (2) hydroxyl group (-OH) must be included since it induces inter-molecular hydrogen bonding, and (3) the set of functional groups cover a wide range of electron-donating character to electron-withdrawing character.

Before calculating the absorption spectra of azobenzene derivatives, each molecular structure must be relaxed to the ground state. First-principles calculation using density functional theory (DFT) was employed in the geometry optimization.

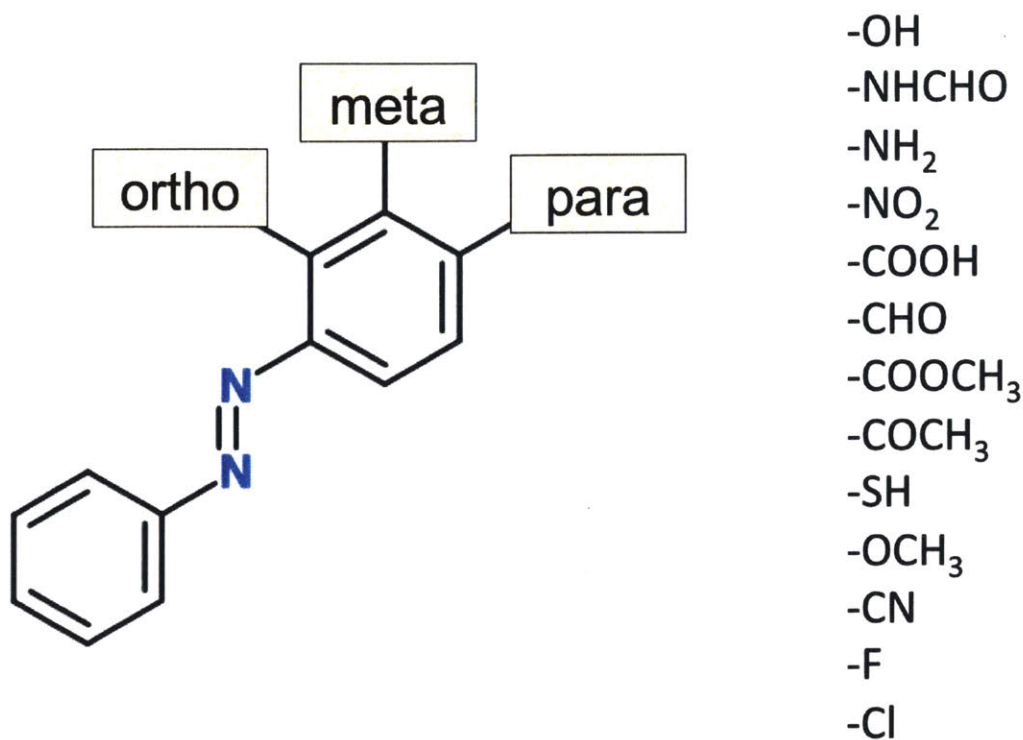


**Figure 3.1** | Schematic diagram of azobenzene functionalization with all studied functional groups

Density functional theory is an *ab initio* method that can quantum mechanically obtain electronic structures of atoms, molecules and crystal structures and thus determine material properties. The derivation of DFT starts with the time-independent  $N$ -electron Schrödinger's equation

$$\hat{H}\Psi = \sum_i^N \left( -\frac{\hbar^2}{2m} \nabla_i^2 + V(\vec{r}_i) + \sum_{j>i}^N \frac{e^2}{4\pi\epsilon_0 |r_i - r_j|} \right) \Psi = E\Psi \quad (3.1)$$

where  $V(\vec{r}_i)$  is the potential energy by the interaction between electron  $i$  and nuclei. Here, the Born-Oppenheimer approximation is applied such that nuclei with substantially larger mass than electrons can be treated as stationary objects.<sup>63</sup> The Hohenberg-Kohn theorem further simplifies

this many-body problem in terms of the ground state electron density  $n(\vec{r})$ . The first part of Hohenberg-Kohn theorem states that for an external potential  $v_{ext}(\vec{r})$ , the ground state electron density  $n(\vec{r})$  is uniquely defined. The second part of Hohenberg-Kohn theorem states that the global minimum energy  $E[n]$  can be determined by the ground state electron density  $n(\vec{r})$ .<sup>64</sup>

The Kohn-Sham equation finally introduces a fictitious system of  $N$  non-interacting electrons that have the same electron density  $n(\vec{r})$ .<sup>65</sup> Since it is a non-interacting system, the Schrödinger equation can be written as a single-particle equation i.e. the Kohn-Sham equation. This single-particle equation is called Kohn-Sham equation:

$$\left( -\frac{\hbar^2}{2m} \nabla^2 + V_s[n(\vec{r})] \right) \varphi_i(\vec{r}) = \varepsilon_i \varphi_i(\vec{r}) \quad (3.2)$$

where  $V_s[n(\vec{r})]$  is the effective single-particle potential which is

$$V_s[n(\vec{r})] = V(\vec{r}) + \int \frac{e^2 n(\vec{r}')}{|\vec{r} - \vec{r}'|} d^3 r' + V_{xc}[n(\vec{r})] \quad (3.3)$$

Here,  $V_{xc}[n(\vec{r})]$  is the exchange-correlation potential that includes all the many-particle interactions. The exchange energy arises due to Pauli's exclusion principle that indistinguishable fermions need to have exchange symmetry and the correlation energy is defined to be the difference between the true single-particle potential and the sum of external potential, Coulomb interaction and exchange potential.<sup>66,67</sup> Approximations on the exchange-correlation potentials are the key to the accuracy of density functional theory. Most commonly used exchange-correlation potential approximations are Local Density Approximation (LDA) and Generalized Gradient Approximation (GGA).<sup>66,68-72</sup>

By solving Equation (3.2), the ground state electron density  $n(\vec{r})$  can be obtained



$$n(\vec{r}) = \sum_{i=1}^N |\varphi_i(\vec{r}')|^2 \quad (3.4)$$

Since the single-particle potential  $V_s[n(\vec{r})]$  in Equation (3.2) is dependent on the ground state electron density  $n(\vec{r})$ , the equation has to be solved “self-consistently” such that the solution of Equation (3.2) satisfies Equation (3.4). Therefore, this method is called a self-consistent field (SCF) method.<sup>73</sup> The minimum energy of the system is obtained by summing the single-particle energies

$$E[n(\vec{r})] = \sum_{i=1}^N \epsilon_i \quad (3.5)$$

Minimizing the DFT-calculated energy of the system as a function of atom positions using numerical optimization algorithms such as steepest descent algorithm and conjugate gradient algorithm leads to geometry optimization of atom positions, i.e. ionic relaxation.<sup>74,75</sup>

Projected Augmented Wave method (PAW) was used to calculate pseudopotential<sup>76,77</sup> and GGA exchange correlation functional was used to solve SCF equations and conjugated gradient algorithm was used to optimize the atomic structures of azobenzene derivatives. In this thesis, plane-wave basis Vienna Ab initio Simulation Package (VASP) was used to perform DFT calculations.<sup>78–81</sup>

### 3.2.2 Theoretical Calculation of Optical Spectra of Azobenzene Derivatives

#### Time-Dependent Density Functional Theory

Optical absorption involves electron-photon interaction that leads to excitation of the valence electron to excited state. Since the Hohenberg-Kohn theorem, the core of density functional theory (DFT), assumes the ground state of the system, i.e. all electrons are in the valence band, DFT cannot properly describe optical processes.<sup>64</sup> Instead, time-dependent density functional theory (TDDFT) can be used to calculate optical properties of materials.

Instead of solving the time-independent Schrödinger's equation as in DFT, TDDFT solves the time-dependent Schrödinger's equation for the many-electron wavefunction  $\Psi(t)$ :

$$\hat{H}(t)\Psi(t) = i \frac{\partial \Psi(t)}{\partial t}, \hat{H}(t) = \hat{T} + \hat{V}_{ee} + \hat{V}_{ext}(t) \quad (3.6)$$

for a given initial wavefunction  $\Psi(0)$ . The kinetic energy operator  $\hat{T}$  and electron-electron repulsion are<sup>82</sup>

$$\hat{T} = -\frac{1}{2} \sum_{i=1}^N \nabla_i^2 \text{ and } \hat{V}_{ee} = \frac{1}{2} \sum_{i \neq j}^N \frac{1}{|r_i - r_j|} \quad (3.7)$$

The external potential  $\hat{V}_{ext}(t)$  represents the electronic potential of photons in optical absorption calculations. Runge and Gross extended the Hohenberg-Kohn theorem to time-dependent systems showing that all observable properties of a many-electron system with initial state  $\Psi(0)$  may be extracted from the one-body time-dependent density  $n(\vec{r}, t)$  alone.<sup>83</sup> Then, a Kohn-Sham (KS) system as in DFT can be formed: an auxiliary system of non-interacting electrons in a one-body potential can be built such that the density of the non-interacting electrons is equal to the

density of the original interacting many-electron system. That is, the density  $n(\vec{r}, t)$  of the interacting system can be obtained from

$$n(\vec{r}, t) = \sum_{j=1}^N |\varphi_j(\vec{r}, t)|^2 \quad (3.8)$$

with KS orbitals  $\varphi_j(\vec{r}, t)$  that satisfy the time-dependent KS equation

$$i \frac{\partial}{\partial t} \varphi_j(\vec{r}, t) = \left[ -\frac{\nabla^2}{2} + v_{KS}[n; \Phi_0](\vec{r}, t) \right] \varphi_j(\vec{r}, t) \quad (3.9)$$

The KS energy functional can be decomposed into three terms as in DFT:

$$v_{KS}[n; \Phi_0](\vec{r}, t) = v_{ext}[n; \Psi_0](\vec{r}, t) + \int d^3r' \frac{n(\vec{r}', t)}{|\vec{r} - \vec{r}'|} + v_{xc}[n; \Psi_0, \Phi_0](\vec{r}, t) \quad (3.10)$$

where  $v_{ext}[n; \Psi_0](\vec{r}, t)$  is the external time-dependent field. The second term corresponds to the electron-electron repulsion and the third term corresponds to the exchange-correlation (xc) potential that has to be approximated with appropriate functionals.  $\Psi_0$  corresponds to the initial state of the interacting system and  $\Phi_0$  corresponds to the initial state of the non-interacting (KS) system.

Almost all functionals in use today have no memory-dependence on  $n(t)$ ; such functionals are called adiabatic. An adiabatic xc functional can be written as

$$v_{xc}^{adia}[n](\vec{r}, t) = v_{xc}^{GS}[n](\vec{r}) \quad (3.11)$$

If the external time-dependence is very slow, this approximation holds true. The adiabatic local density approximation (ALDA) then gives

$$v_{xc}^{ALDA}[n](\vec{r}, t) = v_{xc}^{hom}(n(\vec{r}, t)) \quad (3.12)$$

that the xc potential of homogenous electron gas is used as the xc potential of the KS system.<sup>82</sup>

## Time-Propagation Method

The time-propagation method calculates the time propagation of TDKS orbitals  $\varphi_k(\vec{r}, t)$  following the time-dependent Kohn-Sham equations

$$i \frac{\partial}{\partial t} \varphi_k(\vec{r}, t) = \hat{H}_{KS}[n](\vec{r}, t) \varphi_k(\vec{r}, t) \quad (3.13)$$

from initial condition  $\varphi_k(\vec{r}, t=0) = \varphi_k^{(0)}(\vec{r})$ . The dependence of  $\hat{H}_{KS}[n](\vec{r}, t)$  only on the instantaneous density  $n(\vec{r}, t)$  instead of the whole history shows the adiabatic approximation.<sup>84</sup>

If no perturbation is applied, the time-evolution of the KS wavefunctions is

$$\varphi_k(t) = \varphi_k^{(0)} e^{-ie_k^{(0)} t} \quad (3.14)$$

Otherwise, if we apply a weak delta pulse of a dipole electric field  $\vec{K}$ ,

$$v_{ext}(\vec{r}, t) = -e\vec{r} \cdot \vec{K} \delta(t) = -e\vec{r} \cdot \vec{K} \frac{1}{2\pi} \int_{-\infty}^{\infty} d\omega \exp(i\omega t) \quad (3.15)$$

The KS wavefunctions at  $t = 0^+$  becomes

$$\begin{aligned} \varphi_k(\vec{r}, t=0^+) &= \exp \left\{ -\frac{i}{\hbar} \int_{0^-}^{0^+} dt \left[ \hat{H}_{KS}^{(0)}(t) - e\vec{r} \cdot \vec{K} \delta(t) \right] \right\} \varphi_k(\vec{r}, t=0^-) \\ &= \exp \left( ie\vec{r} \cdot \vec{K} / \hbar \right) \varphi_k(\vec{r}, t=0^-) \end{aligned} \quad (3.16)$$

Equation (3.16) propagate the free oscillations in time following the TDKS equations. Then, from the time-dependent dipole moment

$$\mu(t) = -e \int d^3\vec{r} n(\vec{r}, t) \vec{r} \quad (3.17)$$

and Fourier-transform, the dynamic polarizability tensor  $\alpha(\omega)$  can be obtained.

$$\alpha_{\gamma\delta}(\omega) = \frac{1}{K_\delta} \int_0^\infty dt \left[ \mu_\gamma(t) - \mu_\gamma(0^-) \right] e^{-i\omega t} + \Theta(K_\delta) \quad (3.18)$$

The imaginary part of the diagonal component of the polarizability tensor  $\alpha(\omega)$ , i.e.  $\text{Im}[\alpha_{\delta\delta}(\omega)]$ , is proportional to the absorption spectrum.

Higher order responses are included in the time-propagation calculation; however, if the field  $\vec{K}$  is chosen weak enough, the higher order responses are negligible and hence linear-response is obtained.

In this thesis, real-space ab initio TDDFT package, Octopus code was used to calculate time-propagation of KS orbitals and hence the optical spectra of materials.<sup>85-88</sup>

### Comparison between experimental and theoretically calculated absorption spectra of trans- and cis-Azobenzene

Figure 3.2 shows the comparison between experimentally measured and theoretically calculated absorption spectra of trans- and cis-azobenzene. The TDDFT-calculated spectra were red-shifted possibly due to the underestimation of HOMO-LUMO gap, which is a weakness of density functional theory. However, when the peaks are scissor-shifted to the correct band gap, the peak intensities matched well with the experimental data.

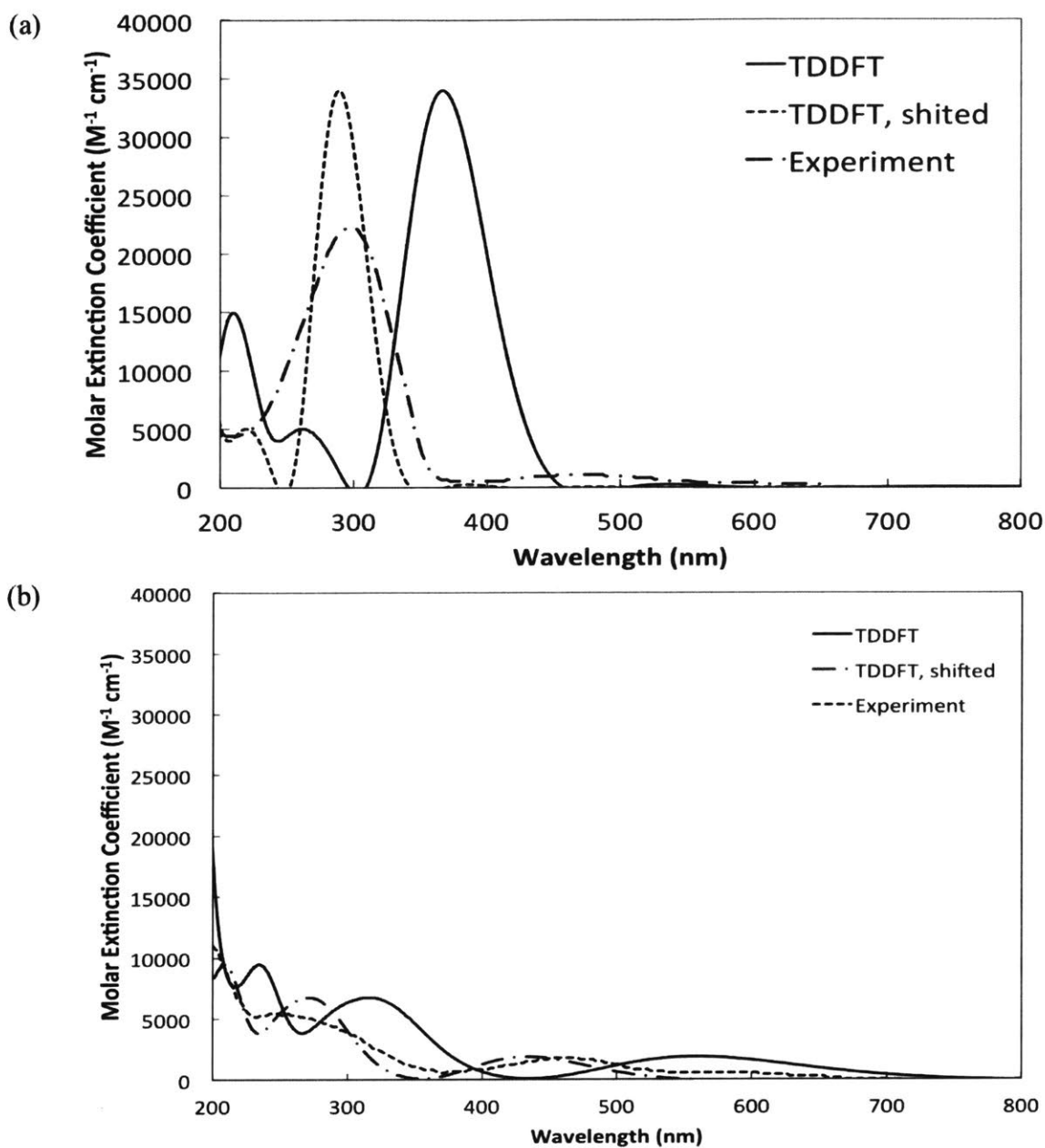


**Figure 3.2** | Comparison between experimentally measured and theoretically calculated spectra of (a) trans-azobenzene and (b) cis-azobenzene. Solid lines represent spectra calculated by TDDFT; Dash-dot lines represent spectra calculated by TDDFT and then shifted to match the band gap; and dashed lines represent experimentally measured absorption spectra of azobenzene.<sup>43</sup>

## Hammett Constant

The Hammett constant in organic chemistry is obtained from the change in the equilibrium constant of benzoic acid ionization (Figure 3.3) with respect to functionalization of the benzene ring of a benzoic acid molecule.<sup>89,90</sup> The Hammett equation is written as

$$\log \frac{K}{K_0} = \sigma \rho \quad (3.19)$$

where  $K$  is the ionization equilibrium constant for substituted benzoic acid,  $K_0$  is the ionization equilibrium constant for pure benzoic acid,  $\sigma$  is the Hammett constant and  $\rho$  is the reaction constant which is 1 for benzoic acid ionization. Large negative  $\sigma$  value means a high electron-donating character of the substitution and large positive  $\sigma$  value means high electron-withdrawing character.

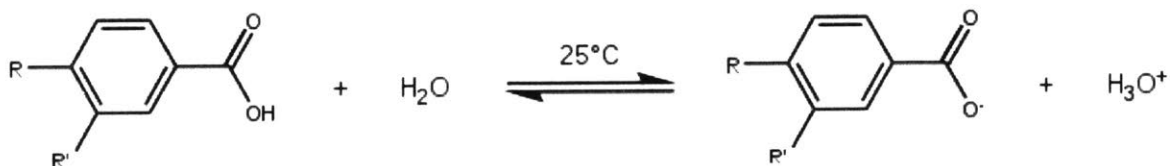


**Figure 3.3** | Ionization of benzoic acid with substituents  $R$  and  $R'$  on para- and meta-position, respectively.

### Absorption Spectra of Azobenzene with NH<sub>2</sub> functionalization on para-position

Among all azobenzene derivatives studied in this thesis, NH<sub>2</sub> functionalization on the para-position has the strongest electron-donating character with Hammett constant  $\sigma = -0.66$ .<sup>91</sup> Therefore, as an example, the absorption spectra of azobenzene with para-NH<sub>2</sub> functionalization calculated using TDDFT time-propagation is shown in Figure 3.4. A strong red-shift of the functionalized trans-azobenzene peak compared to pure azobenzene, from 378 nm to 417 nm, was observed as well as ~30 percent peak intensity increase. Such features in NH<sub>2</sub> functionalized trans-azobenzene spectra indicate that this case would possess a high forward reaction rate from the trans-isomer to cis-isomer. NH<sub>2</sub> functionalized cis-azobenzene spectra also shows a red-shift in peak position and peak intensity increase. Therefore, the backward reaction rate is also higher than pure cis-azobenzene. The photostationary state cis-isomer molar fraction  $x_{cis}$  is then determined by the competing effect of trans- and cis-isomer absorption spectra.



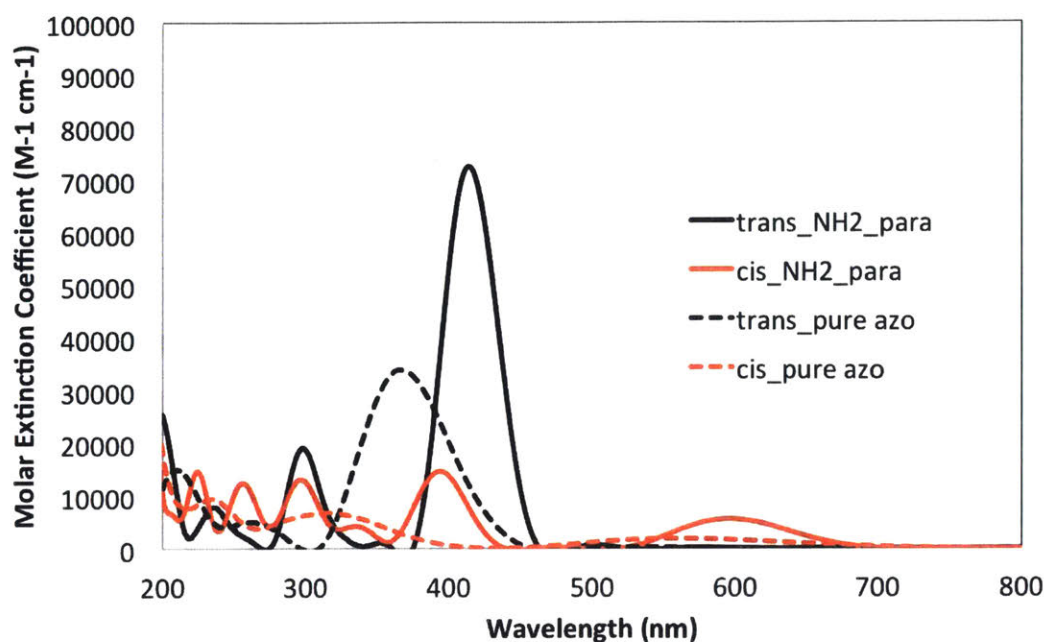


**Figure 3.4** | Absorption spectra of trans-(black) and cis-azobenzene (red) with -NH<sub>2</sub> substitution at para-position. Dotted lines shows the absorption spectra of trans-(black) and cis-azobenzene (red) for comparison.

#### Absorption Spectra of Azobenzene with NO<sub>2</sub> functionalization on para-position

Among all azobenzene derivatives studied in this thesis, NO<sub>2</sub> functionalization on the para-position has the strongest electron-withdrawing character with a Hammett constant  $\sigma = 0.78$ .<sup>91</sup> The absorption spectra of azobenzene with para-NO<sub>2</sub> functionalization calculated using TDDFT is shown in Figure 3.5. The trans-azobenzene absorption peak at 375 nm is red-shifted to 410 nm; however, the peak intensity is decreased compare to the pure-Azo. The absorption peaks of cis-azobenzene are red-shifted and their peak intensities increased after functionalization. As in para-NH<sub>2</sub> functionalized azobenzene, both forward reaction rate and backward reaction rate are increased compare to pure-azobenzene due to the red-shift of peak

positions and peak intensity increases; however, para- NO<sub>2</sub> functionalized azobenzene may exhibit less forward reaction rate than para-NH<sub>2</sub> functionalized azobenzene.

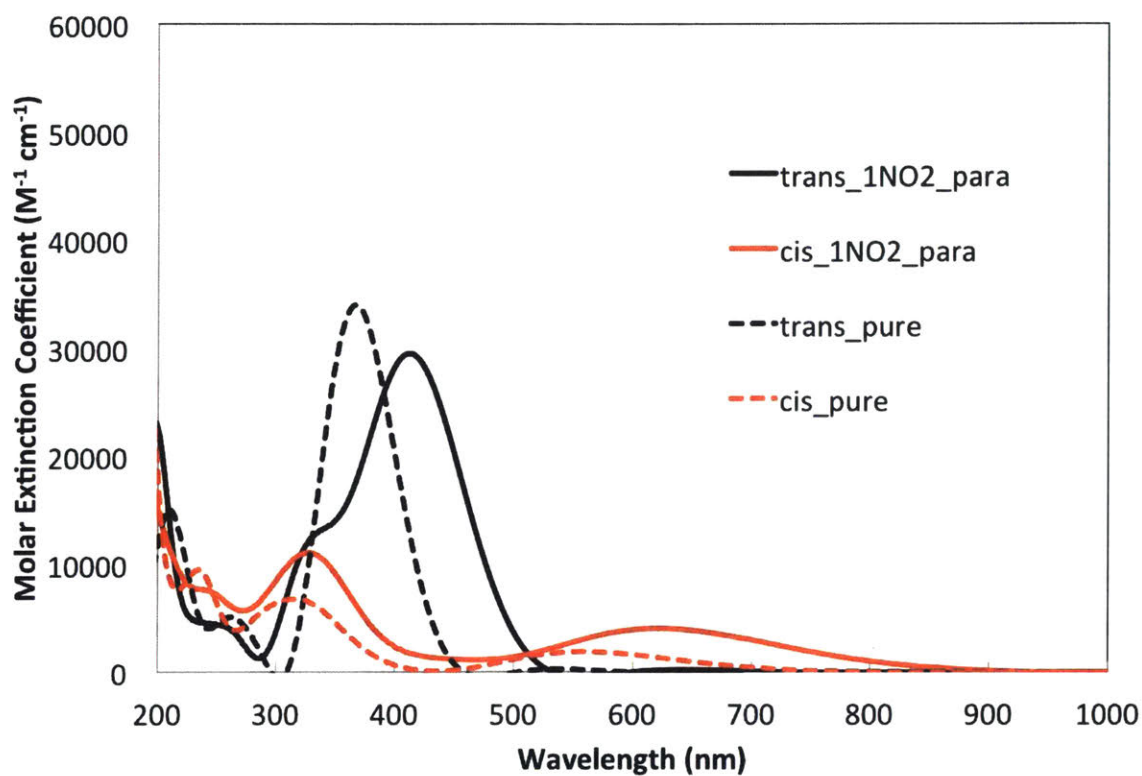


**Figure 3.5** | Absorption spectra of trans-(black) and cis-azobenzene (red) with -NO<sub>2</sub> substitution at para-position. Dotted lines shows the absorption spectra of trans- (black) and cis-azobenzene (red) for comparison.

### 3.3 Photostationary State of Functionalized Azobenzene

Revisit discussion in Chapter 2 to calculate the molar fraction of metastable state

molecule  $x_{metastable,PSS}$  :

$$x_{metastable,PSS} = \frac{k_{forward}}{k_{forward} + k_{backward}} \quad (2.6)$$

The reaction rate constants  $k_{forward}$  and  $k_{backward}$  are obtained from the overlap integrals of the solar spectrum and absorption spectra of ground state and metastable state photoisomer. That is,

$$k_{forward} = \int \frac{I(\lambda)\alpha_{gs}(\lambda)\eta_{gs}(\lambda)}{\frac{hc}{\lambda}} d\lambda \quad (2.7)$$

$$k_{backward} = \int \frac{I(\lambda)\alpha_{metastable}(\lambda)\eta_{metastable}(\lambda)}{\frac{hc}{\lambda}} d\lambda \quad (2.8)$$

where  $I(\lambda)$  is solar spectrum,  $\alpha_i(\lambda)$  is absorption spectrum of material in state  $i$  and  $\eta_i(\lambda)$  is internal quantum efficiency. In this thesis work, NREL AM 1.5 solar spectrum data was used for  $I(\lambda)$  to model STF operation on ground.<sup>92-96</sup>  $\alpha_i(\lambda)$  are calculated using TDDFT time-propagation method. For  $\eta_i(\lambda)$ , values shown in Table 3.1 are used.<sup>97</sup> Kasha's rule states that the excited molecule is thermally relaxed before being quenched to the ground state and hence an appreciable yield of quenching only occurs at the lowest excited state energy level.<sup>98</sup> However, the azobenzene photoisomerization reaction goes through different local minima on the excited state potential energy surface so that the internal quantum efficiency varies for different symmetries of excitation peaks.

**Table 3.1** | Internal quantum efficiency of photoisomerization for trans- and cis-azobenzene. The values are taken from Bortolus et al., *J. Phys. Chem.* 1979, 83, 6, 648-652

peaks	trans-azobenzene	cis-azobenzene
$n \rightarrow \pi^*$ (~439 nm)	0.25	0.56
$\pi \rightarrow \pi^*$ (~317 nm)	0.11	0.27

Photostationary State Molar Fraction  $x_{cis}$  with Respect to the Storage Enthalpy  $\Delta H$

Figure 3.6 shows the correlation between photostationary state molar fraction of cis isomer  $x_{cis}$  and the storage enthalpy  $\Delta H$  for all azobenzene derivatives listed in Figure 3.1. No evident correlation was found between  $x_{cis}$  and  $\Delta H$  indicating that the two values may be optimized separately without affecting each other.

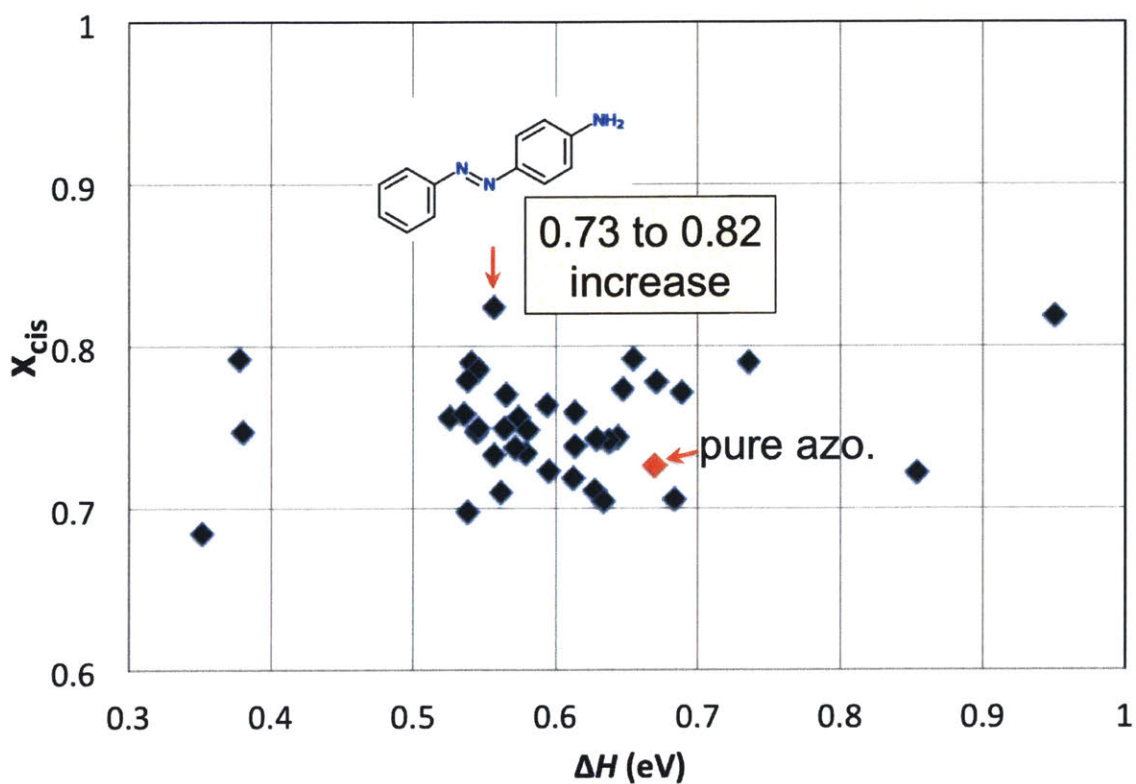


**Figure 3.6** | Photostationary state molar fraction  $x_{cis}$  with respect to the storage enthalpy  $\Delta H$

Photostationary State Molar Fraction  $x_{cis}$  with Respect to the Hammett Constant  $\sigma$

Figure 3.7 shows the correlation between photostationary state molar fraction of cis isomer  $x_{cis}$  and Hammett constant  $\sigma$  of functionalization. A general trend is discovered that the higher the electron-donating character of the functionalization, the higher the  $x_{cis}$  in photostationary state.

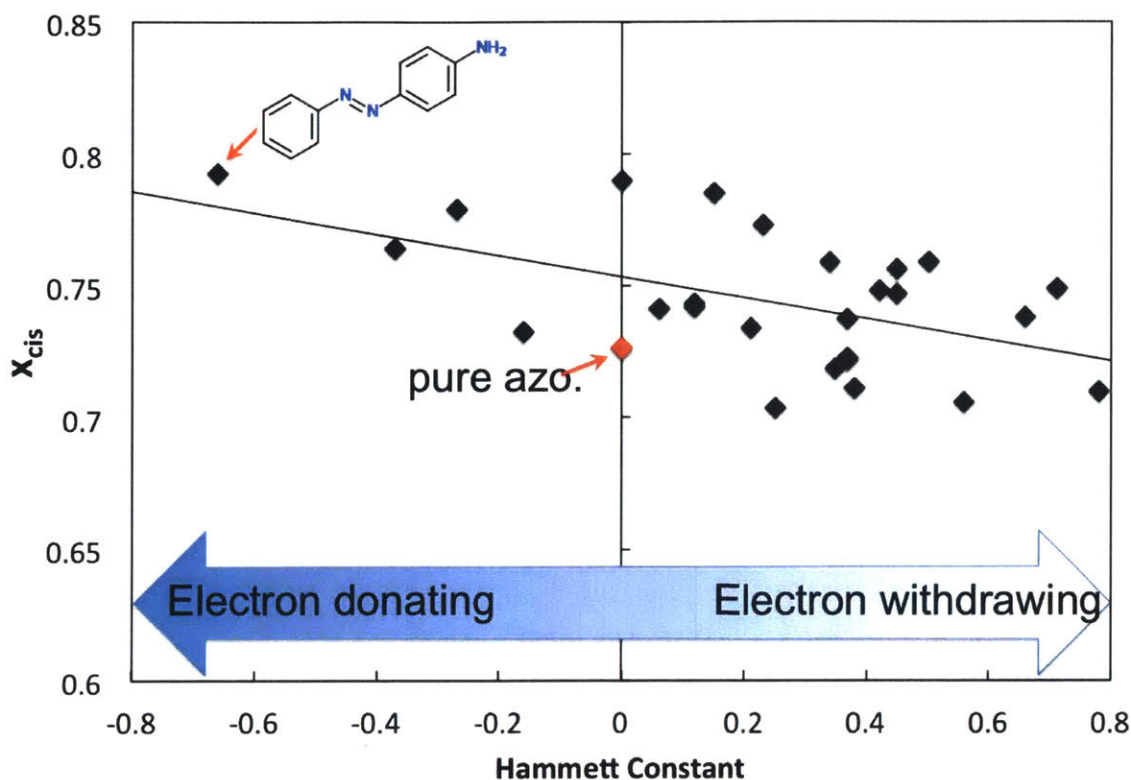


**Figure 3.7** | Photostationary state molar fraction  $x_{cis}$  with respect to the Hammett constant  $\sigma$ . Each black dot corresponds to functionalized azobenzene shown in Figure 3.1. The red dot indicates the pure azobenzene photostationary state  $x_{cis} = 0.73$

#### Theoretical Equivalent of Hammett Constant

Hammett constant  $\sigma$  is a useful parameter to represent electron-donating and electron-withdrawing character of functionalization. However,  $\sigma$  is obtained experimentally; therefore, a theoretical alternative is desired for chemistries with no experimental data, to quantify the electron-donating and electron-withdrawing character.

The extra number of electrons around the N=N double bond  $\Delta N_{N=N}$  is chosen for this study to be such a parameter. The electron density of substituted azobenzene subtracted by the electron density of pure azobenzene was integrated over the two spheres within a Wigner-Seitz radius around the N atoms.<sup>99</sup> Figure 3.8 shows the schematic diagram of the integrated volume.

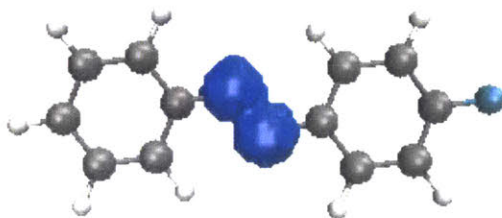


**Figure 3.8** | Integrated volume around N=N double bond. Two spheres with Wigner-Seitz radius around N centers consists the integrated volume.

Figure 3.9 shows the correlation between the extra number of electrons around N=N double bond  $\Delta N_{N=N}$  and the Hammett constants  $\sigma$ . For both trans- and cis-azobenzene derivatives,  $\Delta N_{N=N}$  and  $\sigma$  showed quite strong negative correlation. Therefore,  $\Delta N_{N=N}$  instead of Hammett constant can be used to describe electron-donating and electron-withdrawing characters.

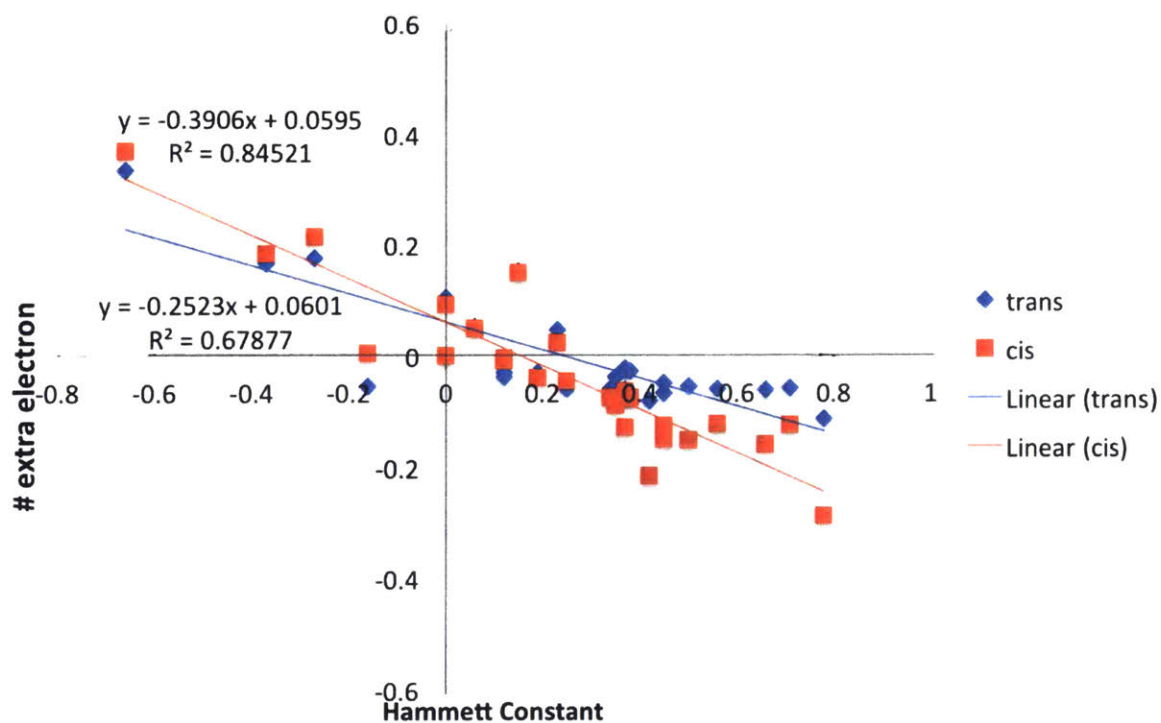


**Figure 3.9** | Correlation between extra number of electrons in N=N bond  $\Delta N_{N=N}$  and the Hammett constants  $\sigma$

Figure 3.10 plots photostationary state cis-isomer molar fraction  $x_{cis}$  in function of # of extra N=N electrons  $\Delta N_{N=N}$ ; which is equivalent to Figure 3.7 using  $\Delta N_{N=N}$  instead of Hammett constant as the x-axis. Hammett constant is only defined for meta- and para-functionalization; but  $\Delta N_{N=N}$  can be defined for ortho-functionalization as well. The black dots in Figure 3.10 show ortho-position functionalized azobenzene derivatives, while the blue dots show meta- and para-position functionalized azobenzene derivatives. Meta- and para-position functionalized azobenzene derivatives show stronger dependence compared to ortho-position functionalized azobenzene derivatives. Such result may be attributed to the bond angle distortion by large functional groups attached to the ortho-position.



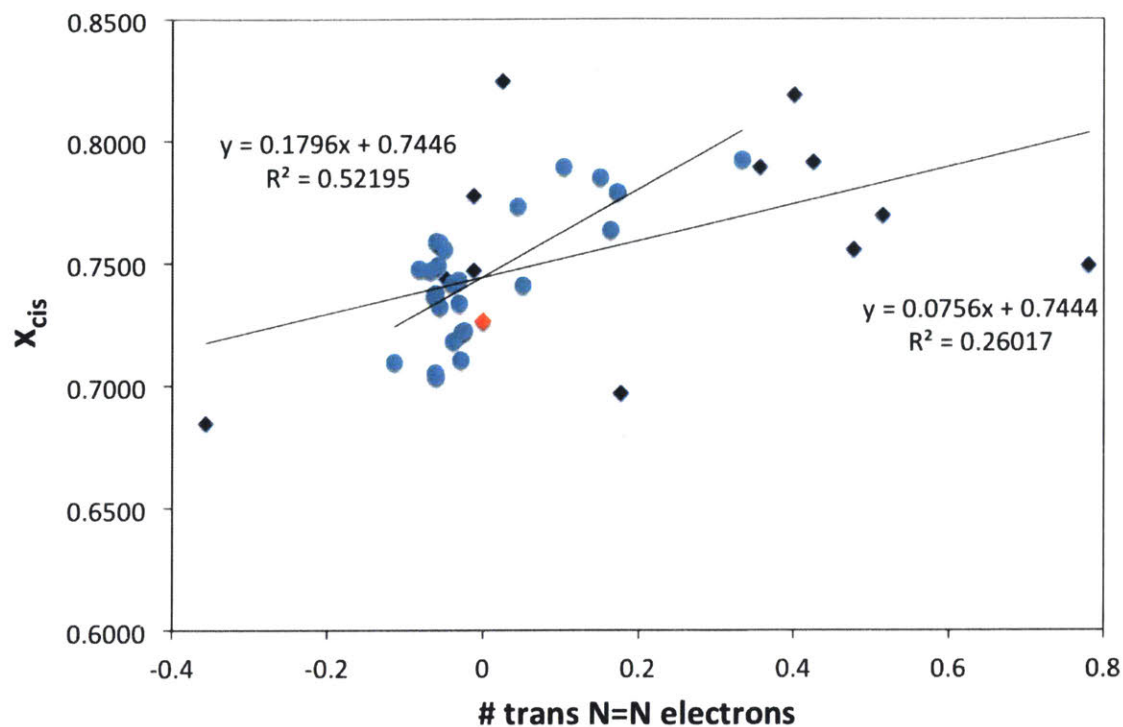


**Figure 3.10** | Photostationary state cis-isomer molar fraction  $x_{cis}$  in function of # of extra N=N electrons  $\Delta N_{N=N}$ . The blue dots indicate meta- and para-functionalized azobenzene. Unmarked black dots indicate ortho-functionalized azobenzene. The blue dots showed stronger correlation between  $x_{cis}$  and  $\Delta N_{N=N}$ , suggesting that steric hindrance in ortho-functionalization led to such irregular correlation between  $x_{cis}$  and  $\Delta N_{N=N}$ .

# Chapter 4

## Geometry Modification of Azobenzene

### 4.1 Motivation for Geometry Modification of Azobenzene

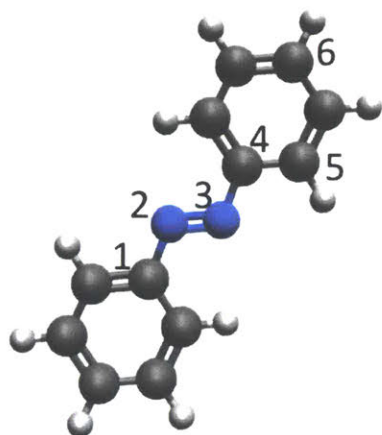
The azobenzene geometry is modified as a result of various chemical treatments such as ortho-functionalization, synthesis of template-Azo structure followed by inter-molecular interaction between packed azobenzene molecules, polymerization and ring structure formation.<sup>2-4,52,61,100</sup> In Chapter 3, functionalizing azobenzene at ortho-position showed less dependence on the electron-donating or electron-withdrawing character compared to functionalizing azobenzene on meta-position or para-position. This result suggests the breakdown of symmetry of azobenzene molecular structure leads to significant change in optical spectra.

So far, the geometry of azobenzene cannot be synthesized in exact desired angles nor be synthesized without chemical effects of supporting structures such as nano-templates and

functional groups. One unique advantage of theory and simulation is that we can explore limits and use that to gain fundamental understanding, which in turn can be used to guide future experiments. In this study, the angles of azobenzene molecules were tailored to focus on the role of geometry on optical spectra and photoisomerization rates of azobenzene-based STFs. The insights gained from this study may be applied to design better azobenzene-based STFs.

## 4.2 Rotational Degrees of Freedom

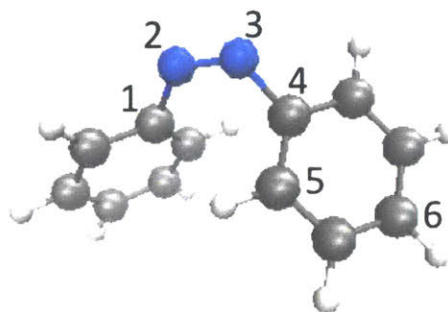
Figure 4.1 shows the rotational degrees of freedom of trans-azobenzene and cis-azobenzene. Point symmetry with respect to the center of N=N double bond is assumed for both trans- and cis-azobenzene. Trans-azobenzene has one bending rotational degree of freedom for angle  $\angle 123 = \angle CNN$  and one twisting rotational degree of freedom for angle  $\angle 2345 = \angle NNCC$ . Cis-azobenzene has two bending rotational degrees of freedom for angle  $\angle 123 = \angle CNN$  and angle  $\angle 346 = \angle NCC$  (benzene ring) as well as two twisting rotational degrees of freedom for angle  $\angle 1234 = \angle CNNC$  and angle  $\angle 2345 = \angle NNCC$ . However, four rotational degrees of freedom yield too many test case combinations. Therefore, in this study, bending angles are fixed at  $\angle 346 = \angle NCC$  (benzene ring) = 0 and  $\angle 123 = \angle CNN = 120$  deg. This assumption is reasonable since for cis-azobenzene, twist angles are relaxed readily so that the bending angles  $\angle 123 = \angle CNN$  and  $\angle 346 = \angle NCC$  (benzene ring) are kept within 5 degrees around the angles defined by the hybridization in relaxed structures of functionalized azobenzene and templated-Azo.



trans azo:

1 bending ( $\angle 123$ )

1 twist ( $\angle 2345$ )



cis azo:

2 bending ( $\angle 123, \angle 346$ )

2 twist ( $\angle 1234, \angle 2345$ )

**Figure 4.1** | Rotational degrees of freedom of trans-azobenzene and cis-azobenzene

### 4.3 Storage Enthalpy and Absorption Spectra of Geometry-Modified Azobenzene

Figure 4.2 shows the ground-state potential energy surface (PES) as a function of the rotational degrees of freedom. The relaxed structures of trans- and cis-azobenzene are marked with red-cross points. For trans-azobenzene, the smaller the bending angle  $\angle 234 = \angle NNC$  is, the higher the ground-state energy is. Also, the smaller the twisting angle  $\angle 2345 = \angle NNCC$ , the more stable the energy of trans-azobenzene. Since trans-isomer is desired to have low energy level, larger bending angle  $\angle 234 = \angle NNC$  and smaller twisting angle  $\angle 2345 = \angle NNCC$  are preferred in terms of ground state energy. On the other hand, high ground-state energy is

preferred for the cis-isomer in order to maintain a large energy storage capacity. Therefore, the smaller the twisting angle  $\angle 2345 = \angle NNCC$  and the other twist angle  $\angle 1234 = \angle CNNC$  near 30 degrees may lead to high storage enthalpy.

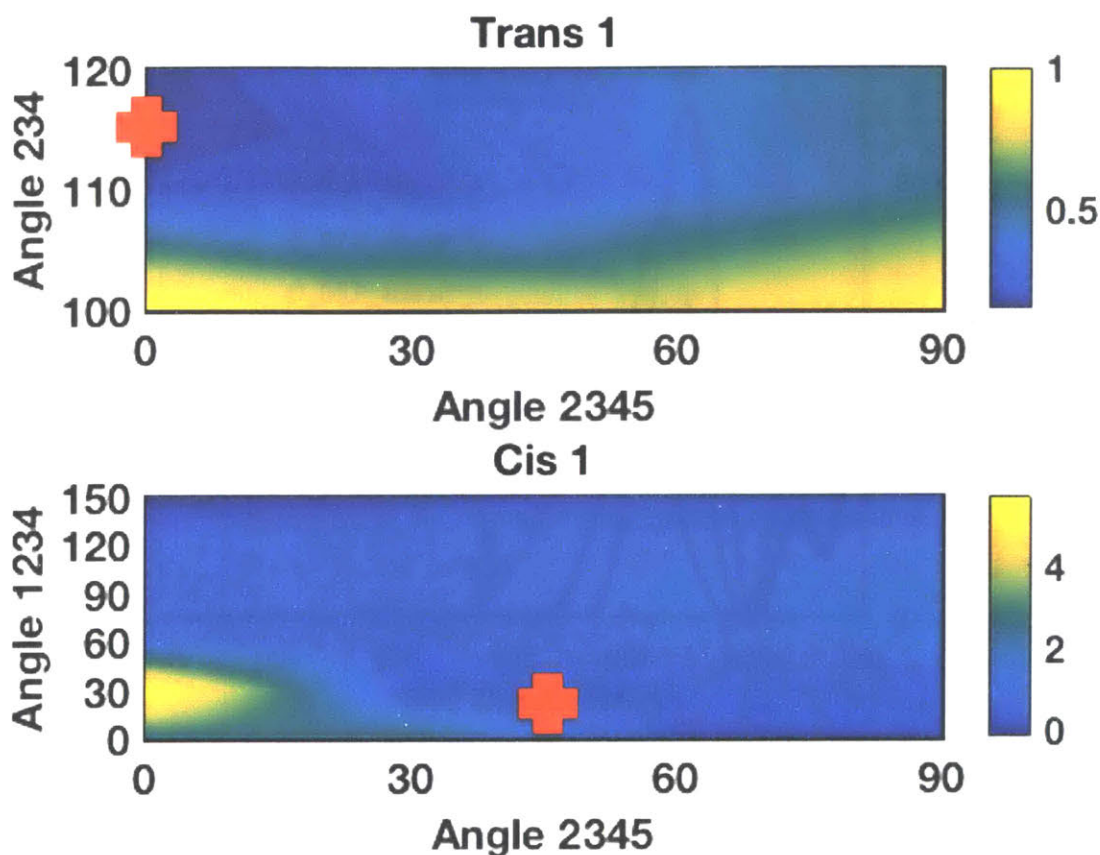


**Figure 4.2** | Ground-state energy surface of (a) trans- and (b) cis-azobenzene in function of geometry. The red-cross point shows the relaxed structure of trans- and cis-azobenzene. Naturally, the relaxed structures are at the global minima. The scale of energy is normalized to the maximum energy in trans-azobenzene potential energy surface in eV.

Figure 4.3 shows absorption spectra of trans-azobenzene with different bending angles calculated by TDDFT as explained in Chapter 3. For planar structures (i.e.  $\angle 2345 = \angle NNCC = 0$

), the  $n \rightarrow \pi^*$  excitation is symmetry forbidden. Hence, for all three structures peak 2 intensities are negligible. Peak 1 which corresponds to  $\pi \rightarrow \pi^*$  is red-shifted but weakened for small bending angles.

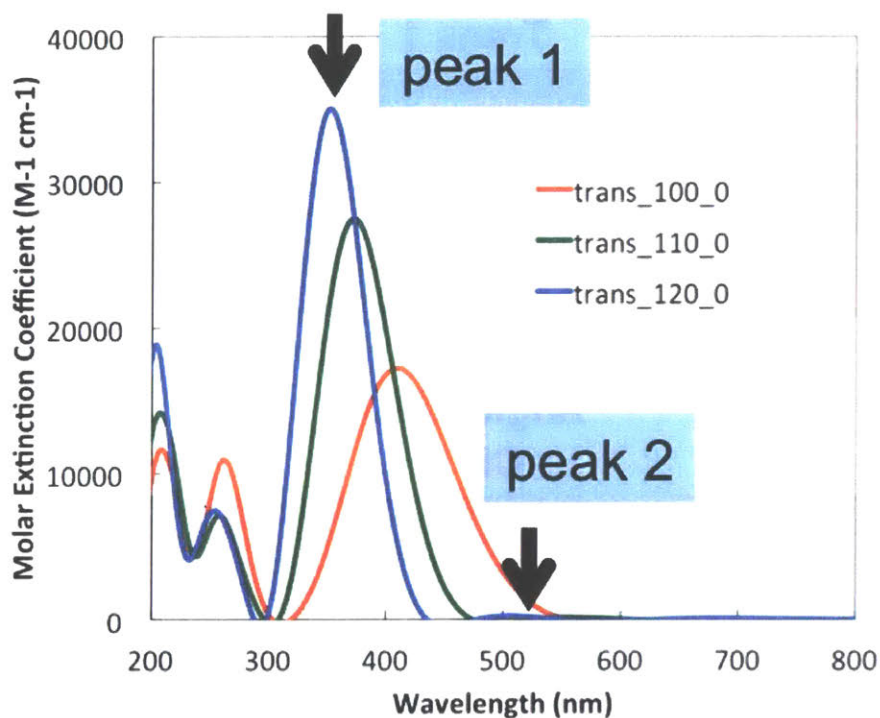


**Figure 4.3** | Absorption Spectra of trans-azobenzene with different bending angles calculated by TDDFT time propagation method. The twist angle  $\angle 2345 = \angle NNCC$  of trans-azobenzene is set to zero for all three examples shown here. Peaks marked with number 1 and 2 correspond to the peak numbering in Figure 4.5 and Figure 4.6. Peak 1 corresponds to  $\pi \rightarrow \pi^*$  excitation and peak 2 corresponds to  $n \rightarrow \pi^*$  excitation.

Figure 4.4 shows absorption spectra of cis-azobenzene with twist angle  $\angle 2345 = \angle NNCC$  fixed to 30 degrees and the other twist angle  $\angle 1234 = \angle CNNC$  is modified

from 0 to 150 degrees with 30 degrees interval. The  $\pi \rightarrow \pi^*$  excitation shows the strongest peak intensity at  $\angle 1234 = \angle CNNC = 150$  degrees, which is a similar structure to trans-azobenzene.

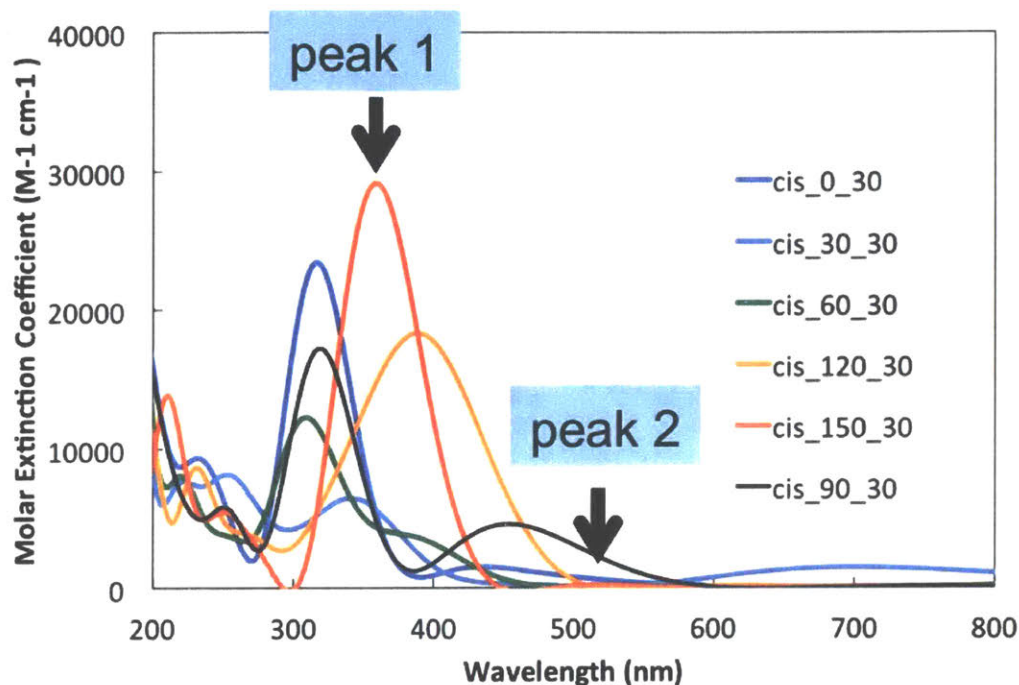


**Figure 4.4** | Absorption Spectra of cis-azobenzene with different twisting angles  $\angle 1234 = \angle CNNC$  calculated by TDDFT time propagation method. The other twist angle  $\angle 2345 = \angle NNCC$  is fixed at 30 degrees. Peaks marked with number 1 and 2 correspond to the peak numbering in Figure 4.5 and Figure 4.6. Peak 1 corresponds to  $\pi \rightarrow \pi^*$  excitation and peak 2 corresponds to  $n \rightarrow \pi^*$  excitation.

Figure 4.5 and Figure 4.6 show the spectral features of trans- and cis-azobenzene in a more systematic way by separately depicting peak position and peak intensity for geometry variations of azobenzene.

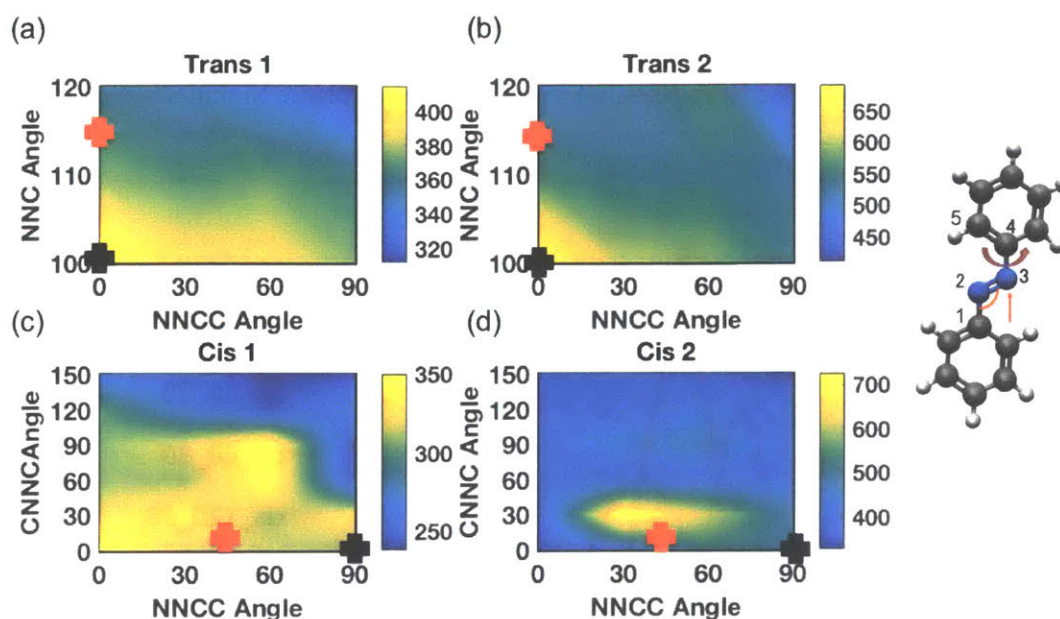


**Figure 4.5** | Peak positions of geometry-modified trans- and cis-azobenzene in color map. For each color map, the right bar indicates the peak position in nm. The angles of relaxed trans- and cis-azobenzene are marked in red-cross, and the geometry that gives the best overlap (maximum overlap for trans-azobenzene and minimum overlap for cis-azobenzene) between solar spectrum and absorption spectrum are marked in black-cross.

Figure 4.5 shows that the best structure for trans-azobenzene absorption peak optimization is  $\angle 234 = \angle NNC = 100^\circ$  since the longer the absorption peak wavelength is, the more the absorption spectra overlaps with the visible range of solar spectrum and hence solar thermal fuel can harvest more optical energy. For cis-azobenzene, it is desired that cis-azobenzene does not absorb light to photoisomerize. Therefore, blue-shift of absorption spectra is preferred; however, the black-cross, which marks the geometry of cis-azobenzene with least overlap between absorption spectra and solar spectrum, shows longer peak wavelength than other structures (Figure 4.5(c) and (d)). This result indicates the peak intensity determined the overlap of cis-azobenzene absorption and solar spectrum.



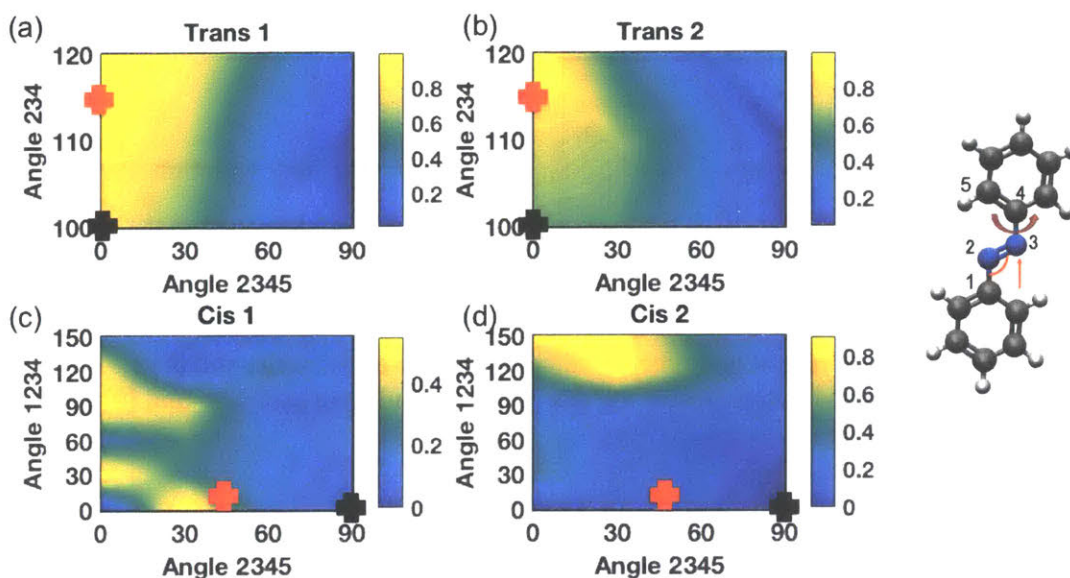


**Figure 4.6** | Peak intensity comparison of geometry-modified trans- and cis-azobenzene in color map. The angles of relaxed trans- and cis-azobenzene are marked in red-cross, and the geometry that gives the most overlap between solar spectrum and absorption spectrum are marked in black-cross.

Figure 4.6 shows the peak intensities for different peaks of geometry modified cis- and trans-azobenzene absorption spectra. Figure 4.6(a) and (b) shows that although absorption peak intensities were higher for larger angle  $\angle 234 = \angle NNC$  but the effect of peak shift in Figure 4.5 dominated the overlap between the trans-azobenzene absorption spectra and solar spectra. Meanwhile, for cis-azobenzene, the peak intensity dominated the overlap between cis-azobenzene absorption spectra and solar spectra. For cis-azobenzene,  $\angle 2345 = \angle MNCC = 90^\circ$  and  $\angle 1234 = \angle CMNC = 0^\circ$  gives the least overlap between absorption spectrum and solar spectrum. This can be attributed to the broken  $\pi$ -bond conjugation between N=N double bond.

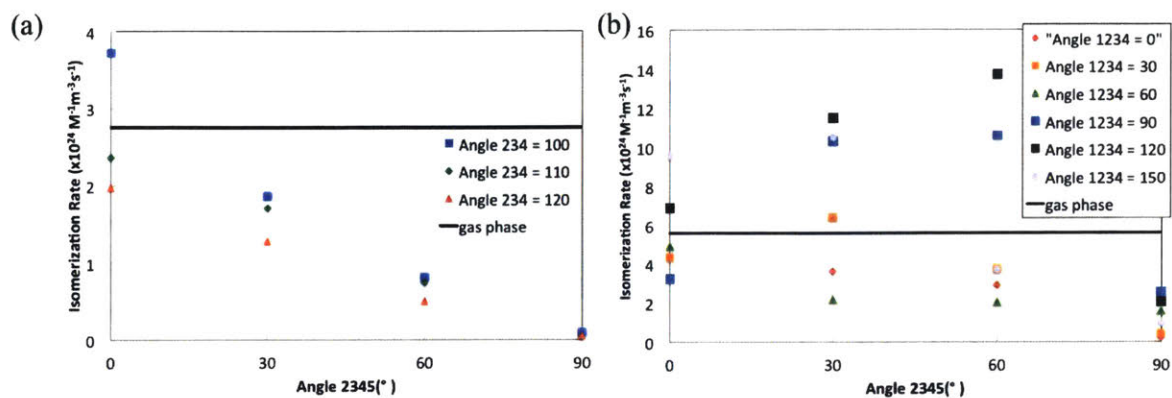


**Figure 4.7** | Isomerization rate of geometry-modified (a) trans-azobenzene and (b) cis-azobenzene. The black solid line indicates the gas phase ground state (a) trans- and (b) cis-azobenzene isomerization rate

The combined effect of peak position and peak intensity is shown in Figure 4.7. The isomerization rates are calculated using Equations (2.7) and (2.8). For trans-azobenzene, the best geometry that yields the highest isomerization rate is  $\angle 234 = \angle NNC = 100^\circ$  and  $\angle 2345 = \angle NVCC = 0^\circ$ ; with this geometry, the isomerization rate is 1.8 times higher the ground state gas phase trans-azobenzene. For cis-azobenzene, the best geometry that yields the lowest isomerization rate is  $\angle 1234 = \angle CNVC = 0^\circ$  and  $\angle 2345 = \angle NVCC = 90^\circ$ , which shows 1/7 reduction of isomerization rate. Combining the best combinations of geometry modified trans- and cis-azobenzene, we get  $x_{cis} = 0.97$  from Equation (2.6).

Figure 4.8 and Figure 4.9 show the extra number of N=N electrons in function of twist or bending angles and their correlation to isomerization rates. Figure 4.8(a) shows that the smaller the bending angle  $\angle 234 = \angle NNC$ , the more the extra number of N=N electrons; and the smaller the twist angle  $\angle 2345 = \angle NVCC$ , the more the extra number of N=N electrons. Figure 4.8(b) shows the correlation between optical isomerization rate and extra number of N=N electrons. As

in Chapter 3, positive correlation between optical isomerization rates and extra number of N=N electrons was observed.

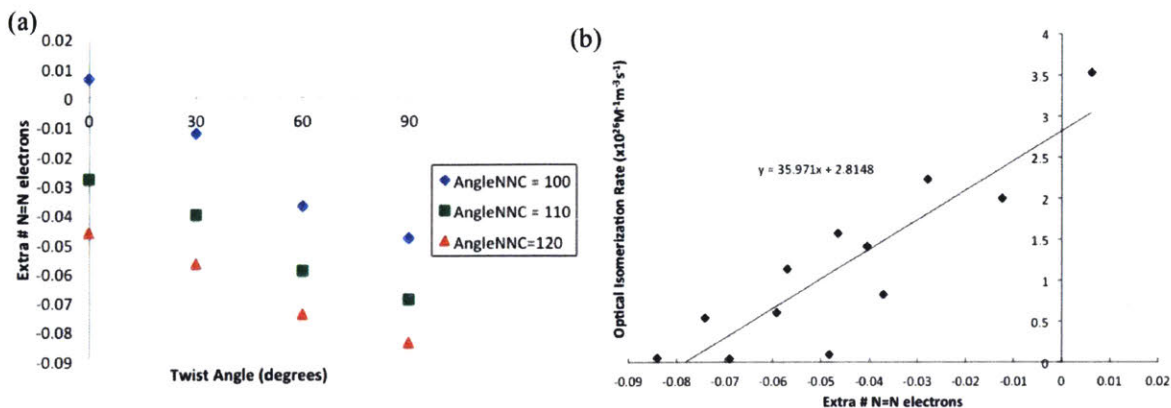


**Figure 4.8** | (a) Extra number of electrons on N=N double bond of trans-azobenzene. (b) Optical isomerization rate of trans-azobenzene in function of extra number of N=N electrons.

Figure 4.9(a) shows that for cis-azobenzene, extra number of N=N electrons has complex relationship with the twist angles as seen in Figure 4.5(c), (d) and Figure 4.6(c), (d). However, when optical isomerization plotted against extra number of N=N electrons, positive correlation was observed again.

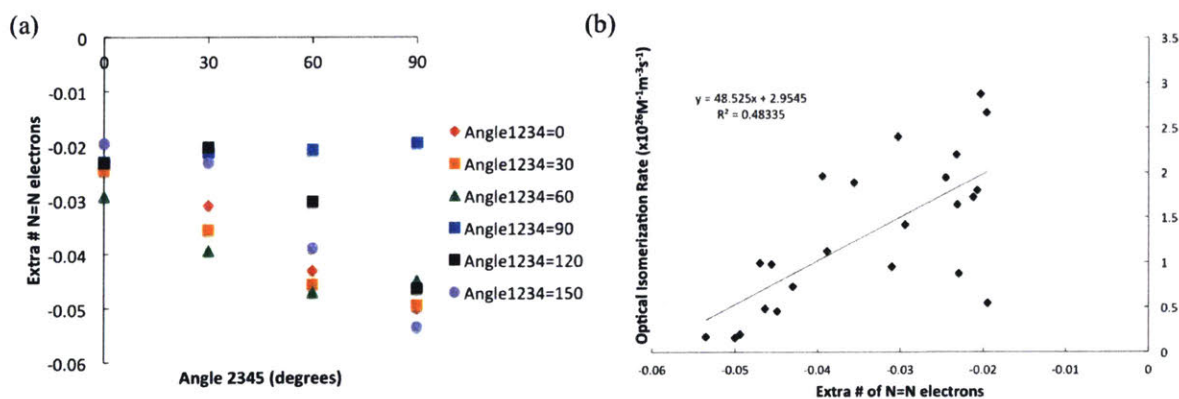


**Figure 4.9** | (a) Extra number of electrons on N=N double bond of cis-azobenzene. (b) Optical isomerization rate of cis-azobenzene in function of extra number of N=N electrons.

# Chapter 5

## Conclusion

Using TDDFT and propagation method, we calculated optical spectra of two molecular designs – functionalization and geometry modification – to study how to optimize photostationary state of azobenzene, a promising candidate material for solar thermal fuels. For both designs, storage enthalpy per molecule ( $\Delta H$ ) and photostationary state cis-azobenzene mole fraction ( $x_{cis}$ ) showed no correlation and hence needed to be optimized separately as expected, since  $\Delta H$  is ground state characteristic while  $x_{cis}$  on the other hand is determined by optical isomerization characteristic associated with both excited state and ground state potential energy surface.

Testing functional groups with various Hammett constant showed negative correlation between the Hammett constant (i.e. the higher the electron withdrawing character) and  $x_{cis}$ . Among this study, 4-aminoazobenzene yielded the highest  $x_{cis}$  improvement from 0.73 (pure azobenzene) to 0.82 (4-aminoazobenzene).

Geometry modification significantly affected optical spectra of trans- and cis-azobenzene and hence their isomerization rates. For trans-azobenzene, within the range of our geometry modification, with optical trans-azobenzene structure, optical isomerization rate was improved by 1.8 than the original gas phase ground state trans-azobenzene. For cis-azobenzene, with optical structure, optical isomerization rate was reduced by 7 times. Combining the two optical isomerization rates of trans- and cis-azobenzene  $x_{cis} = 0.97$  was obtained. For both functionalization and geometry modification showed that the more the extra N=N electrons, the higher the optical isomerization rates were achieved.

This work showed that  $x_{cis}$  of azobenzene can be tuned using functionalization and geometry modification and suggested a few optimal designs. Expanding these ideas, templated-functionalized azobenzene system, which exhibits inherent steric hindrance, may be explored as future work. Such system may tune  $\Delta H$  and  $x_{cis}$  separately, also achieving high energy density by packing many azobenzene molecules in high density as well as by tuning the geometry of trans- and cis-azobenzene on the template due to steric effects.

# Bibliography

1. Kucharski, T. J., Tian, Y., Akbulatov, S. & Boulatov, R. Chemical solutions for the closed-cycle storage of solar energy. *Energy Environ. Sci.* **4**, 4449 (2011).
2. Kolpak, A. M. & Grossman, J. C. Azobenzene-Functionalized Carbon Nanotubes As High-Energy Density Solar Thermal Fuels. *Nano Lett.* **11**, 3156–3162 (2011).
3. Kolpak, A. M. & Grossman, J. C. Hybrid chromophore/template nanostructures: A customizable platform material for solar energy storage and conversion. *J. Chem. Phys.* **138**, 034303 (2013).
4. Kucharski, T. J. *et al.* Templated assembly of photoswitches significantly increases the energy-storage capacity of solar thermal fuels. *Nat. Chem.* **6**, 441–447 (2014).
5. International Energy Agency. Key World Energy Statistics 2017. (2017).
6. Khan, J. & Arsalan, M. H. Solar power technologies for sustainable electricity generation – A review. *Renew. Sustain. Energy Rev.* **55**, 414–425 (2016).
7. Wang, X. *et al.* Polymer Semiconductors for Artificial Photosynthesis: Hydrogen Evolution by Mesoporous Graphitic Carbon Nitride with Visible Light. *J. Am. Chem. Soc.* **131**, 1680–1681 (2009).
8. Dong, L., Feng, Y., Wang, L. & Feng, W. Azobenzene-based solar thermal fuels: design, properties, and applications. *Chem. Soc. Rev.* **47**, 7339–7368 (2018).
9. Weigart, F. Eder's Jahrbuch. *Chem. Abstr.* **4**, 3170
10. Laird, T. *Chem. Ind.* 186 (1978).
11. Jones, G., Reinhardt, T. E. & Bergmark, W. R. Photon energy storage in organic materials— The case of linked anthracenes. *Sol. Energy* **20**, 241–248 (1978).

12. Jones, G., Chiang, S.-H. & Xuan, P. T. Energy storage in organic photoisomers. *J. Photochem.* **10**, 1–18 (1979).
13. Stein, G. *Israel J. Chem.* **14**, 213 (1975).
14. Bowen, E. J. The Photochemistry of Aromatic Hydrocarbon Solutions. in *Advances in Photochemistry* (eds. Noyes, W. A., Hammond, G. S. & Pitts, J. N.) 23–42 (John Wiley & Sons, Inc., 2007). doi:10.1002/9780470133316.ch2
15. Yang, N. C., Shold, D. M. & Kim, B. Chemistry of exciplexes. 5. Photochemistry of anthracene in the presence and absence of dimethylaniline. *J. Am. Chem. Soc.* **98**, 6587–6596 (1976).
16. Waldeck, D. H. Photoisomerization dynamics of stilbenes. *Chem. Rev.* **91**, 415–436 (1991).
17. El'tsov, A. V. *Organic photochromes*. (Consultants Bureau, 1990).
18. Bastianelli, C., Caia, V., Cum, G., Gallo, R. & Mancini, V. Thermal isomerization of photochemically synthesized (Z)-9-styrylacridines. An unusually high enthalpy of Z→E conversion for stilbene-like compounds. *J Chem Soc Perkin Trans 2* 679–683 (1991). doi:10.1039/P29910000679
19. Caia, V., Cum, G., Gallo, R., Mancini, V. & Pitoni, E. A high enthalpy value in thermal isomerization of photosynthesized cis-9-styrylacridines. *Tetrahedron Lett.* **24**, 3903–3904 (1983).
20. Vollhardt, K. P. C. & Weidman, T. W. Synthesis, structure, and photochemistry of tetracarbonyl(fulvalene)diruthenium. Thermally reversible photoisomerization involving carbon-carbon bond activation at a dimetal center. *J. Am. Chem. Soc.* **105**, 1676–1677 (1983).

21. Vollhardt, K. P. C. & Weidman, T. W. Efficient syntheses of new fulvalene-bridged carbonyl complexes of cobalt, ruthenium, chromium, molybdenum, and tungsten. *Organometallics* **3**, 82–86 (1984).
22. Boese, R. *et al.* Photochemistry of (Fulvalene)tetracarbonyldiruthenium and Its Derivatives: Efficient Light Energy Storage Devices. *J. Am. Chem. Soc.* **119**, 6757–6773 (1997).
23. Kanai, Y., Srinivasan, V., Meier, S. K., Vollhardt, K. P. C. & Grossman, J. C. Mechanism of Thermal Reversal of the (Fulvalene)tetracarbonyldiruthenium Photoisomerization: Toward Molecular Solar-Thermal Energy Storage. *Angew. Chem. Int. Ed.* **49**, 8926–8929 (2010).
24. Cho, J. *et al.* Single-Molecule-Resolved Structural Changes Induced by Temperature and Light in Surface-Bound Organometallic Molecules Designed for Energy Storage. *ACS Nano* **5**, 3701–3706 (2011).
25. Hou, Z. *et al.* Switching from Ru to Fe: picosecond IR spectroscopic investigation of the potential of the (fulvalene)tetracarbonyldiiron frame for molecular solar-thermal storage. *Phys. Chem. Chem. Phys.* **15**, 7466 (2013).
26. Börjesson, K. *et al.* Exploring the Potential of Fulvalene Dimetals as Platforms for Molecular Solar Thermal Energy Storage: Computations, Syntheses, Structures, Kinetics, and Catalysis. *Chem. - Eur. J.* **20**, 15587–15604 (2014).
27. Zhu, B., Miljanić, O. Š., Vollhardt, K. P. & West, M. J. Synthesis of 2,2',3,3'-Tetramethyl- and 2,2',3,3'-Tetra-*tert*-butylfulvalene: Attractive- Platforms for Dinuclear Transition Metal Fragments, as Exemplified by ( $\eta^5$ -2,2',3,3'-*t*-Bu<sub>4</sub>C<sub>10</sub>H<sub>4</sub>)M<sub>2</sub>(CO)



- n* (M = Fe, Ru, Os, Mo) and First X-ray Crystal Structures of Fulvalene Diiron and Diosmium Complexes. *Synthesis* 3373–3379 (2005). doi:10.1055/s-2005-918438
28. Hammond, G. S., Wyatt, Peter., DeBoer, C. D. & Turro, N. J. Photosensitized Isomerization Involving Saturated Centers. *J. Am. Chem. Soc.* **86**, 2532–2533 (1964).
29. Philippopoulos, C., Economou, D., Economou, C. & Marangozis, J. Norbornadiene-quadracyclane system in the photochemical conversion and storage of solar energy. *Ind. Eng. Chem. Prod. Res. Dev.* **22**, 627–633 (1983).
30. Ikezawa, Hideo., Kutal, Charles., Yasufuku, Katsutoshi. & Yamazaki, Hiroshi. Direct and sensitized valence photoisomerization of a substituted norbornadiene. Examination of the disparity between singlet- and triplet-state reactivities. *J. Am. Chem. Soc.* **108**, 1589–1594 (1986).
31. Gray, V., Lennartson, A., Ratanalert, P., Börjesson, K. & Moth-Poulsen, K. Diaryl-substituted norbornadienes with red-shifted absorption for molecular solar thermal energy storage. *Chem Commun* **50**, 5330–5332 (2014).
32. Lennartson, A., Roffey, A. & Moth-Poulsen, K. Designing photoswitches for molecular solar thermal energy storage. *Tetrahedron Lett.* **56**, 1457–1465 (2015).
33. Quant, M. *et al.* Low Molecular Weight Norbornadiene Derivatives for Molecular Solar-Thermal Energy Storage. *Chem. - Eur. J.* **22**, 13265–13274 (2016).
34. Goerner, H., Fischer, C., Gierisch, S. & Daub, J. Dihydroazulene/vinylheptafulvene photochromism: effects of substituents, solvent, and temperature in the photorearrangement of dihydroazulenes to vinylheptafulvenes. *J. Phys. Chem.* **97**, 4110–4117 (1993).

35. Görner, H., Fischer, C. & Daub, J. Photoreaction of dihydroazulenes into vinylheptafulvenes: photochromism of nitrophenyl-substituted derivatives. *J. Photochem. Photobiol. Chem.* **85**, 217–224 (1995).
36. Plaquet, A. *et al.* Theoretical investigation of the dynamic first hyperpolarizability of DHA–VHF molecular switches. *New J. Chem.* **33**, 1349 (2009).
37. Lara-Avila, S. *et al.* Light-Triggered Conductance Switching in Single-Molecule Dihydroazulene/Vinylheptafulvene Junctions. *J. Phys. Chem. C* **115**, 18372–18377 (2011).
38. Broman, S. L. *et al.* Dihydroazulene Photoswitch Operating in Sequential Tunneling Regime: Synthesis and Single-Molecule Junction Studies. *Adv. Funct. Mater.* **22**, 4249–4258 (2012).
39. Vlasceanu, A. *et al.* Solar Thermal Energy Storage in a Photochromic Macrocycle. *Chem. - Eur. J.* **22**, 10796–10800 (2016).
40. Skov, A. B. *et al.* Aromaticity-Controlled Energy Storage Capacity of the Dihydroazulene-Vinylheptafulvene Photochromic System. *Chem. - Eur. J.* **22**, 14567–14575 (2016).
41. Vlasceanu, A. *et al.* Photoswitchable Dihydroazulene Macrocycles for Solar Energy Storage: The Effects of Ring Strain. *J. Org. Chem.* **82**, 10398–10407 (2017).
42. Adamson, A. W., Vogler, A., Kunkely, H. & Wachter, R. Photocalorimetry. Enthalpies of photolysis of trans-azobenzene, ferrioxalate and cobaltioxalate ions, chromium hexacarbonyl, and dirhenium decarbonyl. *J. Am. Chem. Soc.* **100**, 1298–1300 (1978).
43. Taoda, H., Hayakawa, K., Kawase, K. & Yamakita, H. Photochemical conversion and storage of solar energy by azobenzene. *J. Chem. Eng. Jpn.* **20**, 265–270 (1987).

44. Yager, K. G. & Barrett, C. J. Novel photo-switching using azobenzene functional materials. *J. Photochem. Photobiol. Chem.* **182**, 250–261 (2006).
45. Masutani, K., Morikawa, M. & Kimizuka, N. A liquid azobenzene derivative as a solvent-free solar thermal fuel. *Chem Commun* **50**, 15803–15806 (2014).
46. Feng, Y. *et al.* Covalent functionalization of graphene by azobenzene with molecular hydrogen bonds for long-term solar thermal storage. *Sci. Rep.* **3**, (2013).
47. Luo, W. *et al.* A high energy density azobenzene/graphene hybrid: a nano-templated platform for solar thermal storage. *J. Mater. Chem. A* **3**, 11787–11795 (2015).
48. Luo, W. *et al.* High-energy, stable and recycled molecular solar thermal storage materials using AZO/graphene hybrids by optimizing hydrogen bonds. *Nanoscale* **7**, 16214–16221 (2015).
49. Feng, W., Li, S., Li, M., Qin, C. & Feng, Y. An energy-dense and thermal-stable bis-azobenzene/hybrid templated assembly for solar thermal fuel. *J. Mater. Chem. A* **4**, 8020–8028 (2016).
50. Zhao, X. *et al.* Controlling Heat Release from a Close-Packed Bisazobenzene-Reduced-Graphene-Oxide Assembly Film for High-Energy Solid-State Photothermal Fuels. *ChemSusChem* **10**, 1395–1404 (2017).
51. Han, G. D. *et al.* Photon energy storage materials with high energy densities based on diacetylene–azobenzene derivatives. *J. Mater. Chem. A* **4**, 16157–16165 (2016).
52. Zhou, H. *et al.* Photoswitching of glass transition temperatures of azobenzene-containing polymers induces reversible solid-to-liquid transitions. *Nat. Chem.* **9**, 145–151 (2017).

53. Ishiba, K. *et al.* Photoliquefiable Ionic Crystals: A Phase Crossover Approach for Photon Energy Storage Materials with Functional Multiplicity. *Angew. Chem. Int. Ed.* **54**, 1532–1536 (2015).
54. Han, G. G. D., Li, H. & Grossman, J. C. Optically-controlled long-term storage and release of thermal energy in phase-change materials. *Nat. Commun.* **8**, (2017).
55. Daley, R. F. & Daley, S. J. *Organic chemistry*. (publisher not identified, 2005).
56. Allen, L. C. Electronegativity is the average one-electron energy of the valence-shell electrons in ground-state free atoms. *J. Am. Chem. Soc.* **111**, 9003–9014 (1989).
57. Mann, J. B., Meek, T. L. & Allen, L. C. Configuration Energies of the Main Group Elements. *J. Am. Chem. Soc.* **122**, 2780–2783 (2000).
58. Mann, J. B., Meek, T. L., Knight, E. T., Capitani, J. F. & Allen, L. C. Configuration Energies of the d-Block Elements. *J. Am. Chem. Soc.* **122**, 5132–5137 (2000).
59. *Compendium of chemical terminology: IUPAC recommendations*. (Blackwell Science, 1997).
60. V. A. Bren, Dubonosov, A. D., Minkin, V. I. & Chernov, V. A. Norbornadiene–quadricyclane — an effective molecular system for the storage of solar energy. *Russ. Chem. Rev.* **60**, 451–469 (1991).
61. Bandara, H. M. D. & Burdette, S. C. Photoisomerization in different classes of azobenzene. *Chem Soc Rev* **41**, 1809–1825 (2012).
62. Hrozhyk, U. A. *et al.* Systematic Study of Absorption Spectra of Donor–Acceptor Azobenzene Mesogenic Structures. *Mol. Cryst. Liq. Cryst.* **489**, 257/[583]-272/[598] (2008).
63. Born, M. & Oppenheimer, R. Zur Quantentheorie der Molekeln. *Ann. Phys.* **389**, 457–484 (1927).

64. Hohenberg, P. & Kohn, W. Inhomogeneous Electron Gas. *Phys. Rev.* **136**, B864–B871 (1964).
65. Kohn, W. & Sham, L. J. Self-Consistent Equations Including Exchange and Correlation Effects. *Phys. Rev.* **140**, A1133–A1138 (1965).
66. Becke, A. D. Density-functional exchange-energy approximation with correct asymptotic behavior. *Phys. Rev. A* **38**, 3098–3100 (1988).
67. Becke, A. D. Density-functional thermochemistry. III. The role of exact exchange. *J. Chem. Phys.* **98**, 5648–5652 (1993).
68. Perdew, J. P. *et al.* Atoms, molecules, solids, and surfaces: Applications of the generalized gradient approximation for exchange and correlation. *Phys. Rev. B* **46**, 6671–6687 (1992).
69. Langreth, D. C. & Mehl, M. J. Beyond the local-density approximation in calculations of ground-state electronic properties. *Phys. Rev. B* **28**, 1809–1834 (1983).
70. Perdew, J. P. & Zunger, A. Self-interaction correction to density-functional approximations for many-electron systems. *Phys. Rev. B* **23**, 5048–5079 (1981).
71. Cole, L. A. & Perdew, J. P. Calculated electron affinities of the elements. *Phys. Rev. A* **25**, 1265–1271 (1982).
72. Perdew, J. P. & Wang, Y. Accurate and simple analytic representation of the electron-gas correlation energy. *Phys. Rev. B* **45**, 13244–13249 (1992).
73. Blinder, S. M. Basic Concepts of Self-Consistent-Field Theory. *Am. J. Phys.* **33**, 431–443 (1965).
74. Kiwiel, K. C. Convergence and efficiency of subgradient methods for quasiconvex minimization. *Math. Program.* **90**, 1–25 (2001).

75. Hestenes, M. R. & Stiefel, E. Methods of conjugate gradients for solving linear systems. *J. Res. Natl. Bur. Stand.* **49**, 409 (1952).
76. Blöchl, P. E. Projector augmented-wave method. *Phys. Rev. B* **50**, 17953–17979 (1994).
77. Kresse, G. From ultrasoft pseudopotentials to the projector augmented-wave method. *Phys. Rev. B* **59**, 1758–1775 (1999).
78. Kresse, G. & Hafner, J. Ab initio molecular dynamics for liquid metals. *Phys. Rev. B* **47**, 558–561 (1993).
79. Kresse, G. & Hafner, J. Ab initio molecular-dynamics simulation of the liquid-metal–amorphous-semiconductor transition in germanium. *Phys. Rev. B* **49**, 14251–14269 (1994).
80. Kresse, G. & Joubert, D. From ultrasoft pseudopotentials to the projector augmented-wave method. *Phys. Rev. B* **59**, 1758–1775 (1999).
81. Kresse, G. & Furthmüller, J. Efficiency of ab-initio total energy calculations for metals and semiconductors using a plane-wave basis set. *Comput. Mater. Sci.* **6**, 15–50 (1996).
82. Gross, E. K. U. & Maitra, N. T. Introduction to TDDFT. in *Fundamentals of Time-Dependent Density Functional Theory* (eds. Marques, M. A. L., Maitra, N. T., Nogueira, F. M. S., Gross, E. K. U. & Rubio, A.) **837**, 53–99 (Springer Berlin Heidelberg, 2012).
83. Runge, E. & Gross, E. K. U. Density-Functional Theory for Time-Dependent Systems. *Phys. Rev. Lett.* **52**, 997–1000 (1984).
84. Strubbe, D. A., Lehtovaara, L., Rubio, A., Marques, M. A. L. & Louie, S. G. Response Functions in TDDFT: Concepts and Implementation. in *Fundamentals of Time-Dependent Density Functional Theory* (eds. Marques, M. A. L., Maitra, N. T., Nogueira, F. M. S., Gross, E. K. U. & Rubio, A.) **837**, 139–166 (Springer Berlin Heidelberg, 2012).

85. Andrade, X. *et al.* Real-space grids and the Octopus code as tools for the development of new simulation approaches for electronic systems. *Phys. Chem. Chem. Phys.* **17**, 31371–31396 (2015).
86. Castro, A. *et al.* octopus: a tool for the application of time-dependent density functional theory. *Phys. Status Solidi B* **243**, 2465–2488 (2006).
87. Marques, M. octopus: a first-principles tool for excited electron–ion dynamics. *Comput. Phys. Commun.* **151**, 60–78 (2003).
88. Castro, A., Marques, M. A. L. & Rubio, A. Propagators for the time-dependent Kohn–Sham equations. *J. Chem. Phys.* **121**, 3425–3433 (2004).
89. Hammett equation (Hammett relation). in *IUPAC Compendium of Chemical Terminology* (eds. Nič, M., Jirát, J., Košata, B., Jenkins, A. & McNaught, A.) (IUPAC, 2009).  
doi:10.1351/goldbook.H02732
90. Keenan, S. L., Peterson, K. P., Peterson, K. & Jacobson, K. Determination of Hammett Equation Rho Constant for the Hydrolysis of p-Nitrophenyl Benzoate Esters. *J. Chem. Educ.* **85**, 558 (2008).
91. Hansch, Corwin., Leo, A. & Taft, R. W. A survey of Hammett substituent constants and resonance and field parameters. *Chem. Rev.* **91**, 165–195 (1991).
92. Gueymard, C. A. Parameterized transmittance model for direct beam and circumsolar spectral irradiance. *Sol. Energy* **71**, 325–346 (2001).
93. Gueymard, C. A. The sun’s total and spectral irradiance for solar energy applications and solar radiation models. *Sol. Energy* **76**, 423–453 (2004).
94. Gueymard, C. A., Myers, D. & Emery, K. Proposed reference irradiance spectra for solar energy systems testing. *Sol. Energy* **73**, 443–467 (2002).

95. Bird, R. E., Hulstrom, R. L. & Lewis, L. J. Terrestrial solar spectral data sets. *Sol. Energy* **30**, 563–573 (1983).
96. Kurtz, S. R. *et al.* Outdoor rating conditions for photovoltaic modules and systems. *Sol. Energy Mater. Sol. Cells* **62**, 379–391 (2000).
97. Bortolus, Pietro. & Monti, Sandra. Cis-trans photoisomerization of azobenzene. Solvent and triplet donors effects. *J. Phys. Chem.* **83**, 648–652 (1979).
98. Kasha, M. Characterization of electronic transitions in complex molecules. *Discuss. Faraday Soc.* **9**, 14 (1950).
99. Wigner, E. & Seitz, F. On the Constitution of Metallic Sodium. *Phys. Rev.* **43**, 804–810 (1933).
100. Durgun, E. & Grossman, J. C. Photoswitchable Molecular Rings for Solar-Thermal Energy Storage. *J. Phys. Chem. Lett.* 854–860 (2013). doi:10.1021/jz301877n